Brainstem Origins of Glutamatergic Innervation of the Rat Hypothalamic Paraventricular Nucleus

Dana R. Ziegler,[1]* Monica R. Edwards,[1] Yvonne M. Ulrich-Lai,[2] James P. Herman,[2] and William E. Cullinan[1]

[1]Department of Biomedical Sciences, Marquette University, Milwaukee, Wisconsin 53201-1881
[2]Department of Psychiatry and Behavioral Neuroscience, University of Cincinnati, Cincinnati, Ohio 45237-0506

ABSTRACT

Multiple lines of evidence document a role for glutamatergic input to the hypothalamic paraventricular nucleus (PVH) in stress-induced activation of the hypothalamic-pituitary-adrenocortical (HPA) axis. However, the neuroanatomical origins of the glutamatergic input have yet to be definitively determined. We have previously shown that vesicular glutamate transporter 2 (VGLUT2) is the predominant VGLUT isoform expressed in the basal forebrain and brainstem, including PVH-projecting regions, and that the PVH is preferentially innervated by VGLUT2-immunoreactive terminals/boutons. The present study employed a dual-labeling approach, combining immunolabeling for a retrograde tract tracer, Fluoro-Gold (FG), with *in situ* hybridization for VGLUT2 mRNA, to map the brainstem and caudal forebrain distribution of glutamatergic PVH-projecting neurons. The present report presents evidence for substantial dual labeling in the periaqueductal gray, caudal portions of the zona incerta and subparafascicular nucleus, and the lateral parabrachial nucleus. The current data also suggest that relatively few PVH-projecting neurons in ascending raphe nuclei, nucleus of the solitary tract, or ventrolateral medulla are VGLUT2 positive. The data reveal multiple brainstem origins of glutamatergic input to PVH that are positioned to play a role in transducing a diverse range of stressful stimuli. J. Comp. Neurol. 520:2369–2394, 2012.

INDEXING TERMS: VGLUT2; Fluoro-Gold; CRH; corticosterone; stress; HPA axis

The hypothalamic-pituitary-adrenocortical (HPA) axis generates glucocorticoid responses to a wide range of stressful stimuli, i.e., challenges that entail a physiological responses and necessitate mobilization of energy stores and adaptive functional changes in the periphery and in the brain. Most stressful stimuli, whether principally physiological challenges (e.g., hypoglycemia, cold, exercise) or primarily "psychogenic" in nature (e.g., predator/conspecific threats, foot shock, restraint, novel environment) involve transduction by CNS pathways that ultimately converge on the hypophysiotropic neurons of the hypothalamic paraventricular nucleus (PVH; Antoni, 1986; Herman et al., 2003; Sawchenko et al., 1996, 2000; Whitnall, 1993; Ziegler and Herman, 2002). Commensurate with this diversity of neuroanatomical pathways encoding different classes of stress-related activity, PVH neurons receive diverse neurochemical input, mediating postsynaptic excitation or inhibition (Herman et al., 2003).

While (nor)adrenergic innervation of the PVH by the A1/C1 and A2/C2 cell groups is well documented as a major excitatory input underlying the transduction of interoceptive stressors (Morilak et al., 2005; Sawchenko et al., 1996, 2000), multiple lines of evidence also point to glutamatergic innervation as an important class of excitatory input to the PVH. Early ultrastructural evidence confirmed glutamate immunopositive synaptic vesicles at asymmetric synapses within the PVH (Bartanusz et al., 2004; Decavel and Van den Pol, 1992; Van den Pol, 1990, 1991), suggesting that glutamate may account for as much as 50% of all synapses within the nucleus (Van den Pol, 1991). This report was followed by studies showing glutamate receptor binding and mRNA and protein expression for glutamate receptor subunits in the PVH (Al-Ghoul et al., 1997; Aubry et al., 1996; Eyigor

Grant sponsor: National Institutes of Health; Grant number: MH69725 (to W.E.C., J.P.H.); Grant number: MH069860 (to J.P.H.); Grant number: DK078906 (to Y.M.U.-L.).

*CORRESPONDENCE TO: Dana R. Ziegler, PhD, Department of Biomedical Sciences, Marquette University, P.O. Box 1881, Milwaukee, WI 53201-1881. E-mail: dana.ziegler@marquette.edu

Received July 15, 2011; Revised September 4, 2011; Accepted January 7, 2012
DOI 10.1002/cne.23043
Published online January 15, 2012 in Wiley Online Library (wileyonlinelibrary.com)

Abbreviations

AHA	anterior hypothalamic area
AHAc	anterior hypothalamic area, central
AHAp	anterior hypothalamic area, posterior
AMBd	nucleus ambiguous, dorsal division
AMBv	nucleus ambiguous, ventral division
AMv	anteromedial
AP	area postrema
APN	anterior pretectal nucleus
AQ	cerebral aqueduct
AQc	cerebral aqueduct, collicular recess
ARH	arcuate nucleus of hypothalamus
B	Barrington's nucleus
bic	brachium of the inferior colliculus
bsc	brachium of the superior colliculus
C	central canal
CENT2b	central lobule, lubule II, sublobule b
CENT3a	central lobule, lubule III, sublobule a
cic	inferior colliculus commissure
COM	periaqueductal gray, commissural nucleus
cpd	cerebral peduncle
csc	superior colliculus commissure
CSl	central superior nucleus raphé, lateral
CSm	central superior nucleus raphé, medial
cst	corticospinal tract
CU	cuneate nucleus
cuf	cuneate fascicle
CUL	culmen
CUN	cuneiform nucleus
dcn	deep cerebellar nuclei
DMX	dorsal motor nucleus of the vagus nerve
DR	nucleus raphe dorsal
DTN	dorsal tegmental nucleus
ECU	external cuneate nucleus
em	external medullary lamina thalamus
EW	Edinger-Westphal nucleus
FF	fields of forel
Fr	fasciculus retroflexus
fx	fornix
GRN	gigantocellular reticular nucleus
Hab	habenular nuclei
hbc	habenular commissure
IC	inferior colliculus
ICc	inferior colliculus, central nucleus
ICd	inferior colliculus, dorsal nucleus
ICe	inferior colliculus, external nucleus
icp	inferior cerebellar peduncle
IF	interfascicular nucleus raphé
IGL	intergeniculate leaflet (of LG)
IO	inferior olivary complex
IPN	interpeduncular nucleus
IVn	trochlear nerve
KF	Kölliker-Fuse subnucleus (of PB)
LC	locus coeruleus
LDT	laterodorsal tegmental nucleus
LGd	lateral geniculate, dorsal
LGvl	lateral geniculate, ventrolateral
LGvm	lateral geniculate, ventromedial
LHA	lateral hypothalamic area
LHAjp	lateral hypothalamic area, juxtaparaventric.
LHAjvv	lateral hypothal. area, juxtaventromedial
LHAp	lateral hypothalamic area, posterior region
LIN	linear nucleus medulla
ll	lateral lemniscus
LM	lateral mammillary nucleus
LP	lateral posterior nucleus of thalamus
LRNm	lateral reticular nucleus, magnocellular
LRNp	lateral reticular nucleus, parvicellular
LTN	lateral tegmental nucleus
MARN	magnocellular reticular nucleus, ventral
mcp	middle cerebellar peduncle
MDRNv	medullary reticular nucleus, ventral
ME	median eminence
MEex	median eminence, external lamina
MEin	median eminence, internal lamina
MEV	midbrain trigeminal nucleus
MGd	medial geniculate complex, dorsal
MGl	medial geniculate complex, lateral
MGm	medial geniculate complex, medial
MGv	medial geniculate complex, ventral
MH	medial habenula
ml	medial lemniscus
mlf	medial longitudinal fascicule
MM	medial mammillary nucleus, body
MMme	medial mammillary nucleus, medial
moV	motor root of the trigeminal nerve
mp	mammillary peduncle
MPT	medial pretectal area
MR	nucleus raphe median
MRNm	midbrain reticular nucleus, magnocellular
mtg	mammillotegmental tract
MV	medial vestibular nucleus
ND	nucleus of Darkschewitsch
NId	nucleus incertus, dorsal
NIS	nucleus intercalatus
NLLd	nucleus of the lateral lemniscus, dorsal
NLLh	nucleus of the lateral lemniscus, horizontal
NLLv	nucleus of the lateral lemniscus, ventral
NOT	nucleus of the optic tract
NPC	nucleus of the posterior commissure
NR	nucleus of Roller
NTB	nucleus of the trapezoid body
NTSce	nucleus of the solitary tract, central
NTSco	nucleus of the solitary tract, commissural
NTSge	nucleus of the solitary tract, gelatinous
NTSl	nucleus of the solitary tract, lateral
NTSm	nucleus of the solitary tract, medial
OP	olivary pretectal nucleus
opt	optic tract
PAG	periaqueductal gray
PAGd	periaqueductal gray, dorsal division
PAGm	periaqueductal gray, medial division
PAGrl	periaqueductal gray, rostrolateral division
PAGrm	periaqueductal gray, rostromedial division
PAGvl	periaqueductal gray, ventrolateral division
PARN	parvicellular reticular nucleus
PAS	parasolitary nucleus
PAT	paratrigeminal nucleus
PBlc	parabrachial nucleus, central lateral
PBld	parabrachial nucleus, dorsal lateral
PBle	parabrachial nucleus, external lateral
PBls	parabrachial nucleus, superior lateral
PBlv	parabrachial nucleus, ventral lateral
PBmm	parabrachial nucleus, medial medial
pc	posterior commissure
PCG	pontine central gray
PF	parafascicular nucleus thalamus
PG	pontine gray
PGRNl	paragigantocellular reticular nucleus, lateral
PH	posterior hypothalamic nucleus
pm	principal mammillary tract
PMR	paramedian reticular nucleus
PO	posterior complex thalamus
POL	posterior limiting nucleus thalamus
POR	periolivary nuclei
PP	peripeduncular nucleus
PPN	pedunculopontine nucleus
PPT	posterior pretectal nucleus
PRC	precommissural nucleus, periaqueductal gray
PRNc	pontine reticular nucleus, caudal
PRNr	pontine reticular nucleus, rostral
PSV	principal sensory nucleus of the trigeminal
PVH	paraventricular nucleus of hypothalamus
PVHdp	PVH dorsal parvicellular
PVHlp	PVH lateral parvicellular
PVHmpd	PVH medial parvicellular, dorsal part
PVHmpv	PVH medial parvicellular, ventral part
PVHpml	PVH posterior magnocellular, lateral
PVHpv	PVH periventricular part
PVi	periventricular hypothalamus, intermediate
py	pyramid
RE	reunions nucleus of thalamus
RH	rhomboid nucleus of thalamus
RL	rostral linear nucleus raphe
RM	nucleus raphe magnus
RMVE	rostral medullary velum
RN	red nucleus
RO	nucleus raphe obscurus
RPA	nucleus raphe pallidus
RPO	nucleus raphe pontis
Rust	rubrospinal tract
SBPV	subparaventricular zone of hypothalamus
SCdg	superior colliculus, deep gray layer
SCdw	superior colliculus, deep white layer
SCig	superior colliculus, intermediate gray layer, a–c

et al., 2001, 2005; Herman et al., 2000; Khan et al., 2000; Kiss et al., 1996; Mateos et al., 1998; Oliver et al., 1996; Petralia and Wenthold, 1996; Sato et al., 1993; Tasker et al., 1998; Van den Pol et al., 1994; Ziegler et al., 2005). In addition to these anatomical data, electrophysiological data from cultured slices have documented functional excitatory responses of PVH neurons to glutamatergic input (Bartanusz et al., 2004; Boudaba et al., 1997; Daftary et al., 1998, 2000; Van den Pol et al., 1990, 1996; Wuarin and Dudek, 1991) and in vivo studies involving glutamate or glutamate receptor antagonist microinjections in the PVH led to stimulation/inhibition of the HPA axis at the level of corticotropin-releasing hormone (CRH), adrenocorticotropic hormone (ACTH), and corticosterone secretion (Cole and Sawchenko, 2002).

Previous tract-tracing studies have catalogued a set of CNS regions with direct projections to the PVH, as reviewed in detail elsewhere (Herman et al., 2003; Sawchenko et al., 1996, 2000; Swanson, 1987; Swanson and Sawchenko, 1983; Ziegler and Herman, 2002). However, until recently, it was not technically feasible to determine which PVH afferent regions supply glutamatergic input because of the lack of specific markers for glutamatergic neurons prior to the recent identification of the vesicular glutamate transporter protein family (VGLUT1–3). One earlier study investigated the origins of glutamatergic innervation of the PVH using retrograde tracing with ^{3}H-D-aspartate (Csaki et al., 2000), based on its ostensible uptake at the terminal by high-affinity glutamate/aspartate reuptake transporters on the presynaptic membrane (Rothstein et al., 1994; Storm-Mathisen et al., 1995), and reported putative glutamatergic PVH-projecting neurons in several forebrain areas. However, the significance of this report is limited by 1) lack of cases with tracer placement filling the medial parvocellular (adenohypophysiotropic) subdivision; 2) lack of retrograde labeling in brainstem regions; and, most importantly, 3) uncertainty regarding tracer uptake by glutamatergic terminals following reports of possible uptake by γ-aminobutyric acid (GABA)-ergic neurons (Furuta et al., 1997a,b; Kugler and Schmitt, 1999; Rothstein et al., 1994; Velaz-Faircloth et al., 1996).

The VGLUT1 and VGLUT2 genes were cloned and identified as brain homologs of peripheral inorganic phosphate transporters that (in the CNS) show specific vesicular transport of glutamate (i.e., much lower transport of aspartate and no transport of GABA or glycine), with the same electrochemical biophysical profile (transport driven by an ATP-dependent electrochemical gradient) previously reported in vitro for the putative vesicular glutamate transporter protein isolated from brain homogenate (Aihara et al., 2000; Bai et al., 2001; Bellocchio et al., 1998, 2000; Fremeau et al., 2001; Hayashi et al., 2001; Ni et al., 1994, 1995; Ozkan and Ueda, 1998; Takamori et al., 2000; Varoqui et al., 2002), and are specifically localized to the vesicular compartment (Bellocchio et al., 1998, 2000; Fujiyama et al., 2001; Hayashi et al., 2001; Takamori et al., 2000). Furthermore, dual-labeling tests for the expression of VGLUT1 and VGLUT2 in GABAergic neuron cell bodies or terminals in cultured neurons or in the hypothalamus have shown that these markers do not colocalize (Fujiyama et al., 2001; Ziegler et al., 2002), and ultrastructural analyses confirm localization selectively to asymmetric (putatively excitatory)

Abbreviations (Continued)

SCop	superior colliculus, optic layer
SCsg	superior colliculus, superficial gray layer
SCzo	superior colliculus, zonal layer
SCO	subcommissural organ
scp	superior cerebellar peduncle
sctv	ventral spinal cerebellar tract
SGN	suprageniculate nucleus
SLC	subceruleus nucleus
SLD	sublaterodorsal nucleus
smd	supramammillary decussation
SNc	substantia nigra, compacta
SNr	substantia nigra, reticulata
SOCl	superior olivary complex, lateral
SOCm	superior olivary complex, medial
SPF	subparafascicular nucleus thalamus
SPFpl	SPF, parvicellular, lateral
SPFpm	SPF, parvicellular, medial
SPIV	spinal vestibular nucleus
sptV	spinal tract of the trigeminal
SPVC	spinal nucleus of the trigeminal, central
SPVI	spinal nucleus of the trigeminal, interpolar
SPVO	spinal nucleus of the trigeminal, oral
SUMl	supramammillary nucleus, lateral
SUMm	supramammillary nucleus, medial
SUT	supratrigeminal nucleus
SUV	superior vestibular nucleus
sV	sensory root of the trigeminal nerve
tb	trapezoid body
Thal	thalamus
TMv	tuberomammillary nucleus, ventral
TRN	tegmental reticular nucleus, pontine gray
ts	solitary tract
tsp	tectospinal pathway
TUsv	tuberal nucleus hypothal., subparaventricular
V3h	3rd ventricle, hypothalamic
V3m	3rd ventricle, mammillary recess
V4	fourth ventricle proper
VCOa	ventral cochlear nucleus, anterior
VIIn	facial nerve
VIIIn	vestibulocochlear nerve
Vma	motor nucleus of the trigeminal nerve, magno.
VMH	ventromedial nucleus of hypothalamus
VMHa	VMH, anterior part
Vn	trigeminal nerve
Vpc	motor nucleus of the trigeminal nerve, parvi.
VPL	ventral posterolateral nucleus thalamus
VPM	ventral posteromedial nucleus thalamus
VTA	ventral tegmental area
VTN	ventral tegmental nucleus
XII	hypoglossal nucleus
z	nucleus z
ZI	zona incerta

synapses (Bellocchio et al., 1998; Boulland et al., 2009; Fujiyama et al., 2001; Kaneko et al., 2002). Initial studies of the gross CNS distributions of VGLUT1/2 mRNA revealed largely nonoverlapping and complementary distributions, with VGLUT1 predominating in the telencephalon and cerebellar cortex, whereas VGLUT2 is the dominant isoform in the diencephalon, brainstem, and deep cerebellar nuclei (Aihara et al., 2000; Bellocchio et al., 1998; Fremeau et al., 2001; Hisano et al., 2002; Kaneko and Fujiyama, 2002; Ni et al., 1994, 1995).

More recently, neuroanatomically detailed investigations of VGLUT2 mRNA distribution have documented VGLUT2 mRNA in almost all brain regions known to contain PVH-projecting neurons, including medial and lateral septum, some preoptic nuclei, most hypothalamic nuclei, thalamic paraventricular nucleus, periaqueductal gray, laterodorsal tegmental nucleus, parabrachial area, and pedunculopontine nucleus and within the A1/A2 noradrenergic cell groups and C1–C3 noradrenergic cell groups (Barroso-Chinea et al., 2007; Collin et al., 2003; Hisano et al., 2000; Hrabovszky et al., 2005; Hur and Zaborszky, 2005; Kiss et al., 2007; Lin et al., 2003; Stornetta et al., 2002; Wang and Morales, 2009; Ziegler et al., 2002). Moreover, immunohistochemical studies have confirmed the presence of VGLUT2-immunoreactive terminals and/or synapses in the PVH, and dual-labeling analyses have found VGLUT2-positive boutons in apposition to CRH-positive PVH neurons (Wittmann et al., 2005; Ziegler et al., 2005). In contrast, the PVH lacks innervation by VGLUT1-immunoreactive fibers or terminals (Kaneko et al., 2002; Ziegler et al., 2005), consistent with the low-to-negative VGLUT1 mRNA expression in brain regions known to project the PVH (i.e., in basal forebrain, diencephalon, and brainstem; see references cited above).

Thus, with the emergence of VGLUT2 as the dominant glutamatergic marker expressed within brain regions known to project to the PVH, mapping the neuroantomical distribution of glutamatergic PVH-projecting neurons is achievable through a dual-label approach combining retrograde tract tracing and *in situ* hybridization for VGLUT2 as a neuronal soma marker. Accordingly, our group has performed such an analysis of forebrain sources of glutamatergic input to the PVH (Ulrich-Lai et al., 2011).

Although the literature on brainstem input to the PVH has focused largely on ascending serotonergic and catechoaminergic cell groups, recent evidence has highlighted the presence of VGLUT2 mRNA expression within brainstem PVH-projecting regions (present data and above references). The present investigation employed the same dual-label approach to identify the distribution of brainstem glutamatergic PVH projecting neurons. It should be acknowledged that a minor portion of glutamatergic innervation to the PVH appears to be mediated by the more recently identified VGLUT3 isoform. VGLUT3 has been well-characterized as a specific vesicular transporter of glutamate (Fremeau et al., 2002; Gras et al., 2002; Schafer et al., 2002; Takamori et al., 2002). Although we have observed VGLUT3-immunoreactive fibers and terminals within the PVH (Ziegler and Cullinan, unpublished observations), VGLUT3 mRNA is expressed in only three of the numerous known PVH-projecting regions: the bed nucleus of the stria terminalis (BNST), the posterior hypothalamic nucleus, and the raphe nuclei and at moderate to low intensities (Gras et al., 2002; Herzog et al., 2004; Schafer et al., 2002). Thus, given the clear dominance of the VGLUT2 isoform in almost all brainstem PVH-projecting regions, we have used VGLUT2 as a marker for brainstem glutamatergic PVH-projecting neurons in the present study.

MATERIALS AND METHODS

Animals and tissue processing

Adult male Sprague-Dawley rats (250–350 g) from Harlan (Indianapolis, IN) were used for the single- and dual-labeling studies. Rats were housed in a vivarium colony room with controlled temperature and humidity, with food and water available ad libitum. All animal procedures conformed to NIH guidelines and were approved by the Institutional Care and Use Committee of Marquette University. For single-label hybridization (VGLUT2 mRNA), rats were killed by rapid decapitation, with brains frozen in −40°C isopentane, sectioned on a cryostat at 14 μm, and stored at −20°C until further processing. For Fluoro-Gold (FG) single-immunolabeling and for dual-labeling studies, rats were deeply anesthetized with a lethal overdose of anesthetic and perfused transcardially with 100 ml of 0.1 M sodium phosphate-buffered saline (PBS; pH 7.4) followed by 250 ml of 4% paraformaldehyde in 0.1 M sodium phosphate buffer. Prior to use, PBS was incubated at 37°C for 1 hour with the addition of 0.01% (v/v) diethylpyrocarbonate (DEPC) to inactivate any RNAse present and autoclaved. Paraformaldehyde was prepared using commercially supplied nuclease-free ddH_2O (VWR). Brains were removed and postfixed overnight and cryoprotected with 30% sucrose in paraformaldehyde for 2–3 days before sectioning on a freezing microtome at 40 μm. Sections were collected into DEPC-treated PBS in a 1:6 series and transferred to cryostorage until further processing of selected cases. Cryoprotection and storage at −20°C were achieved by using a solution of 30% sucrose, 30% v/v ethylene glycol, 10% polyvinylpyrrolidone, in PB (pH 7.4), known to maintain structural integrity of the tissue and to preserve antigen detection (Watson et al., 1986).

Stereotaxic surgery and FG microinjection

Rats were anesthetized with a ketamine/xylazine mixture (50 mg/ml ketamine; 10 mg/ml xylazine), and a rectangular window was cut from the skull area overlying the targeted region. A glass micropipette was back-filled with a 3% solution of FG (Fluorochrome, Denver, CO) in sterile saline (0.9%) and placed in the PVH (−1.8 mm caudal to bregma, 0.3 mm lateral from midline, −7.5 mm ventral to dural surface). FG was iontophoretically delivered to the PVH for 3 minutes at 2.5 μA, 7 seconds on/off, with a constant current device stimulator (model 51413; Precision Current Source; Stoelting Co., Wood Dale, IL). The micropipette was left in place for 10 minutes before withdrawal to minimize diffusion of tracer. The skull window was packed with Gelfoam (Pharmacia and Upjohn, Kalamazoo, MI), and the scalp was closed with surgical staples. Rats were prophylactically administered 10 μg/kg buprenorphine for pain relief and were given a 10–14-day postoperative survival period to allow for recovery and sufficient retrograde transport of tracer.

Single-label immunohistochemistry for FG

The first series of sections for each case was processed through immunohistochemistry alone to assess the accuracy of FG placements and to verify effective retrograde transport to the predicted regions. Specifically, sections were removed from cryoprotectant solution and rinsed several times in PBS and preincubated and permeabilized in the diluent solution used for antibody incubations: PBS containing 0.3% v/v Triton X-100 and 0.25% carrageenan (Sigma, St. Louis, MO) at room temperature for 15 minutes. Sections were then transferred to the primary antibody incubation, rabbit anti-FG (catalog No. 52-9600, Fluorochrome; immunogen = FG, unconjugated), diluted 1:10,000 in diluent solution, and incubated for 2–3 days at 4°C with mild agitation on an orbital shaker. After primary incubation, sections were washed in PBS (5 × 1 minute) to remove unbound primary antibody and then incubated with a biotinylated secondary antibody: 1:200 biotinylated goat anti-rabbit (catalog No. BA-1000; Vector Laboratories, Burlingame, CA) for 1 hour at room temperature. Sections were washed in PBS (5 × 1 minute) and incubated with avidin-biotin peroxidase complex (ABC Elite Kit;, Vector Laboratories) diluted 1:500 in PBS with 0.3% v/v Triton X-100 for 1 hour at room temperature. Sections were washed once again in PBS (5 × 1 minute) and subsequently reacted in chromogenic staining solution containing 0.5 mg/ml diaminobenzidene (DAB) and 0.03% hydrogen peroxide in 0.1 M PB. Reactions proceeded for up to 30 minutes to allow maximally strong signal to develop. Finally, stained sections were mounted on polylysine-coated slides, air dried, dehydrated through ascending ethanols, immersed in xylene, and coverslipped with Polymount (Polysciences, Warrington, PA) for microscopic examination. The specificity of the primary antibody was confirmed by the lack of any staining in sections from rats that did not receive FG injections (not shown). Specificity of the secondary antibody and subsequent steps was confirmed by the lack of any staining in sections processed with omission of primary antibody (not shown).

Riboprobe preparation/hybridization histochemistry

Riboprobes for VGLUT2 (originally named *DNPI*, 734 bp, 5′ cloned into pGEM-T EZ vector) were generated using standard in vitro transcription methodology, with SP6 polymerase and ^{35}S-UTP as the radiolabel (Perkin-Elmer/NEN, Boston, MA) as described by Ziegler et al. (2002). Briefly, plasmid was linearized with PvuII at a site in the vector external to the VGLUT2 cDNA insert, thus yielding antisense riboprobe representing the entire 734-bp 5′-cloned segment of the VGLUT2 gene. Salt/ethanol precipitation was used to separate riboprobe from free nucleotides. Incorporation of ^{35}S-UTP was assessed by a yield of $>10^6$ CPM/μl of isolated and resuspended probe. The specificity of the VGLUT2 riboprobe has been characterized previously (Ziegler et al., 2002). Slides were pretreated with a 10-minute fixation in 4% paraformaldehyde (phosphate-buffered), glycine block (0.2% in PBS), acetylation (0.25% acetic anhydride in 0.1 M triethanolamine, pH 8.0); dehydration/delipidation through ascending ethanols, 100% chloroform, and a final 100% ethanol; and air dried for >30 minutes before hybridization. Stored riboprobe was preheated at 55–60°C for >5 minutes prior to dilution into hybridization buffer containing 0.02 M dithiothreitol (DTT). Slides were hybridized with diluted probe yielding 10^6 CPM/50 μl per slides, coverslipped, and incubated overnight at 55–60°C. After hybridization incubation, coverslips were removed and slides processed through a posttreatment protocol consisting of SSC rinse steps, treatment with 15 μg/100 ml ribonuclease A (RNAse A) for 30 minutes at 37°C, SSC rinses, a high-stringency wash step in 0.2× SSC at 60°C for 1 hour, SSC rinses, ethanol dehydration, and air drying prior to film exposure on Kodak Biomax MR film for 2 weeks.

Combined *in situ* hybridization (VGLUT2) and immunohistochemistry (FG)

For dual-labeling for FG and VGLUT2 mRNA, several series of free-floating sections were sequentially processed through *in situ* hybridization, followed by immunohistochemistry. For VGLUT2 hybridization, cRNA riboprobe

was synthesized and isolated as described above. The hybridization protocol for these free-floating sections was modified from the procedures described above for slide-mounted cryostat-cut, postfixed sections. Prehybridization treatment was performed as follows: sections were removed from the cryostorage solution in an excess volume of DEPC-treated PBS, rinsed for 2 × 1 minute in DEPC-treated PBS, permeabilized for 15 minutes in DEPC-treated PBS containing 0.3% (v/v) Triton X-100, and rinsed for 2 × 1 minute in DEPC-treated PBS before transfer into the riboprobe incubation. As described above, riboprobe was preheated to hybridization temperature (55–60°C) for >5 minutes before dilution into commercial hybridization buffer (Amresco, Solon, OH), containing 0.02 M DTT. Each series of sections was incubated in 4 ml DTT-containing hybridization buffer with riboprobe diluted to yield an incubation concentration of 10^6 CPM per section. Incubations occurred in securely capped glass vials in an incubation oven at 55–60°C overnight. After the hybridization incubation, sections were processed through a posttreatment protocol. Specifically, sections were rinsed for 5 × 1 minute in room temperature 2× SSC, transferred to glass vials containing 5 ml of 20 mg/100 ml RNAse A solution, incubated for 30 minutes at 37°C, rinsed for 2 × 1 minute in 2× SSC, rinsed for 3 × 1 minute in 0.2× SSC, subjected to a high-stringency wash in 0.2× SSC for 1 hour at 60°C, rinsed for 1 × 1 minute in 02× SSC, and rinsed for 4 × 1 minute in PBS before proceeding to the FG immunohistochemistry procedure, which was performed as described above. After FG immunohistochemistry and rinses in PBS, sections were mounted onto polylysine-coated slides, air dried, cleaned through an ascending series of ethanols, and air dried.

Autoradiographic processing

Slides with mounted sections from the combined hybridization-immunolabeling procedure were first exposed to Kodak Biomax MR autoradiographic film for 7 days to confirm successful VGLUT2 hybridization. Slides were then dipped in undiluted Ilford K5D autoradiographic emulsion (Polysciences) that had been prewarmed and stabilized at 42°C in total darkness, air dried for 3–4 hours, packaged into sealed slides boxes, and stored (exposed) at 4°C for 7 days. After 7 days, slide boxes were removed from the cold and allowed >2 hours to equilibrate to room temperature prior to opening and development. Slides were then immersed in Kodak D-19 developer solution for 2 minutes, rinsed in ddH_2O, and immersed in Kodak Rapid Fix for 3 minutes. Solutions were chilled to 18°C prior to use. Slides were extensively rinsed in ddH_2O, dehydrated through ethanols, transferred to xylene, and coverslipped in Polymount. Later, during analysis of dual labeling, selected slides had coverslips removed in xylene, rehydrated through descending ethanols, lightly counterstained with 0.5% cresyl violet (Sigma-Aldrich, St. Louis, MO), dehydrated, and recoverslipped with Permount.

Data analysis

Neurons classified as FG-positive were clearly and specifically labeled by a brownish precipitate that was typically evident as granular staining within the soma. In some cases, soma were homogenously filled with DAB reaction product. FG labeling of the proximal portions of dendrites was occasionally found. The neuroanatomical pattern of FG^+ neuronal labeling was consistent with previous retrograde studies. VGLUT2 mRNA signal was analyzed by visual inspection for grain clustering over FG^+ neuronal soma. For each section analyzed, the background grain density was assessed by surveying the grain density over neuronal cell bodies (identified by Nissl staining) lacking specific labeling for VGLUT2 mRNA. Background grain density was assessed as both grains per cell body and grains per unit area corresponding to typical cross-sectional profile typical of FG^+ neurons using a reticule micrometer. This grain density was comparable if not identical to both nearby white matter and adjacent nonsomatic territory (neuropil) within the $VGLUT2^+$ region being analyzed. A neuron was classified as $VGLUT2^+$ if the density of grains overlying the cell body was at least threefold higher than the observed background density. Manual grain counting over neuronal soma was performed for all such soma in which the overlying grain density did not clearly exceed three times threshold. Figure 3 presents examples of neurons that were dually labeled as well as examples of those positive for FG or VGLUT2 alone.

Abbreviations and nomenclature for coronal plates are derived from Swanson (2004). For all sections per case, raw data were recorded by plotting the location of observed FG^+ neurons onto photocopies of a closely matching plate from Swanson's brain map atlas (Swanson, 2004), with each such plate integrating observations from one to three sections. Raw data were used as a reference in composing the schematic illustrations in Figures 4–6, which represent selected rostrocaudal levels (most of the levels examined with substantial numbers of FG^+ neurons). The coronal schematic panels were prepared by modifying and annotating Adobe Illustrator files derived from the CD-ROM from the brain map atlas. The neuroanatomical locations of single- and dual-labeled neurons were determined and plotted on schematic plates based on spatially interpolating from the discernible borders of the nuclei and available anatomical

landmarks in the section, aided by the light counterstain applied (cresyl violet).

After this neuroanatomical mapping of single- and dual-labeled FG^+ neurons, a quantitative summary was performed, with data presented in Table 1 for four brain regions that showed the highest degree of single or dual labeling. For each listed region and for each case, all sections spanning the same rostral-caudal levels were included in a summation of total FG^+ neurons and total $FG^+/VGLUT2^+$ neurons, with dual labeling also reported as percentage of total FG^+ neurons. All sections included in this analysis were evenly spaced and derived from a single 1:6 series. Because of this spacing and a section thickness of 40 μm, we have assumed a lack of double-counting error in the Table 1 data. Table 1 does not include any extrapolation from this analysis to an estimate of the true total numbers of FG^+ neurons or total number of dual-labeled neurons per region, primarily because of uncertainty about a valid correction factor for undercounting of FG^+ neurons. Specifically, each section typically contained some partial profiles of FG^+ neuronal cell bodies visible within analyzed sections, which were excluded from the analysis, i.e., excluded from total FG^+ neuron counts and assessment of VGLUT2 expression (Table 1, Figs. 4–6). Thus, given the unlikelihood of any overcounting errors along with some degree of undercounting of total FG^+ neurons in each section, as we have indicated in Table 1, the true total neurons numbers are probably greater than sixfold times the numbers listed, which are based on summation across the analyzed sections from the 1:6 series.

TABLE 1.

Quantitative Summary of Dual Labeling for Fluoro-Gold (FG) and VGLUT2 mRNA in Major Afferents[1]

Region	Total No. FG^+	No. $FG^+/VGLUT2^+$	$FG^+/VGLUT2^+$ (%)	N
Periaqueductal gray, rostral (PRC, m, rm, COM)				
Case 478	27	9	33.3	4
Case 491	48	12	25.0	5
Case 495	87	40	46.0	5
Periaqueductal gray, caudal PAGvl				
Case 478	13	8	61.5	3
Case 491	13	5	38.5	2
Case 495	51	16	31.4	2
Lateral parabrachial nucleus (PBl)				
Case 478	36	9	25.0	5
Case 491	90	32	35.6	3
Case 495	149	87	58.4	4
Kölliker-Fuse subnucleus (KF)				
Case 478	5	0	0.0	4
Case 491	36	15	41.7	3
Case 495	46	22	47.8	4

[1]Regional designations for periaqueductal gray (PAG): rostral PAG level was defined as including the precommissural nucleus (PRC), medial (m) and rostromedial (rm) PAG subdivisions, and the commissural nucleus (COM), as defined in the brain map of Swanson (2004), rostrocaudally spanning atlas levels 34–38 as illustrated in Figures 4A–D, 5A–D, 6A–D, i.e., rostral to the level where the canonical column organization emerges (dorsal, dorsolateral, lateral, ventrolateral columns). Caudal PAGvl refers to a caudal portion of the ventrolateral column, with data collected from atlas levels 47–48 (Figs. 4E,F, 5E,F, 6E,F). Lateral parabrachial data were collected from atlas levels 47–51 (Figs. 4E–H, 5E–H, 6E–H). Kölliker-Fuse data were collected from atlas levels 47–49 (Figs. 4E–G, 5E–G, 6E–G). N (last column), numbers of sections analyzed per case. Note that total numbers of neurons (FG^+ only or dually labeled) reflect summation across all analyzed sections. True totals per brain region (extrapolating across all six section series) are likely greater than sixfold times the totals given. Experimental factors precluded an exact quantitative extrapolation (see Materials and Methods).

Autoradiograph and photomicrograph processing

Image processing details for film autoradiograph images of VGLUT2 mRNA distribution (Fig. 1) and for brightfield photomicrographs of single or dual-labeled sections (Fig. 3) are as follows. All film images in Figure 1 were digitally captured with identical camera and digital input parameters (aperture, magnification, brightness, and contrast) using a Pulnix CCD camera and digital output unit, connected to an Apple desktop computer equipped with a Scion video card and running NIH Image software (National Institutes of Health). Adobe Photoshop CS2 (Adobe Systems, San Jose, CA) was then used to crop and resize images uniformly and to apply identical brightness/contrast adjustments. Individual images were then assembled and annotated in Adobe Illustrator CS2. Photographic images of sections in Figure 3 were captured with a Zeiss Axioplan 2 light microscope equipped with a Spot digital camera and Spot software (Diagnostic Instruments, Sterling Heights, MI), which was used for initial image adjustments for sharpness, brightness, and contrast. Individual images were then cropped, resized, and further adjusted for brightness, contrast, and color in Adobe Photoshop CS2. Finally, images were assembled and annotated in Adobe Illustrator CS2.

RESULTS

Technical considerations: single-labeling vs. combined dual-labeling procedures

Before examining single- and dual-labeling data, some brief observations follow here regarding the sensitivity of FG^+ immunolabeling (or VGLUT2 mRNA detection) in single- vs. dual-labeling experiments. As noted in Materials and Methods, because of concern about the potential for compromised FG immnostaining following *in situ* hybridization, an entire series of sections from the FG cases was processed through FG immunohistochemistry alone. No differences were detected in the numbers or neuroanatomical distributions of FG^+ neurons between the two

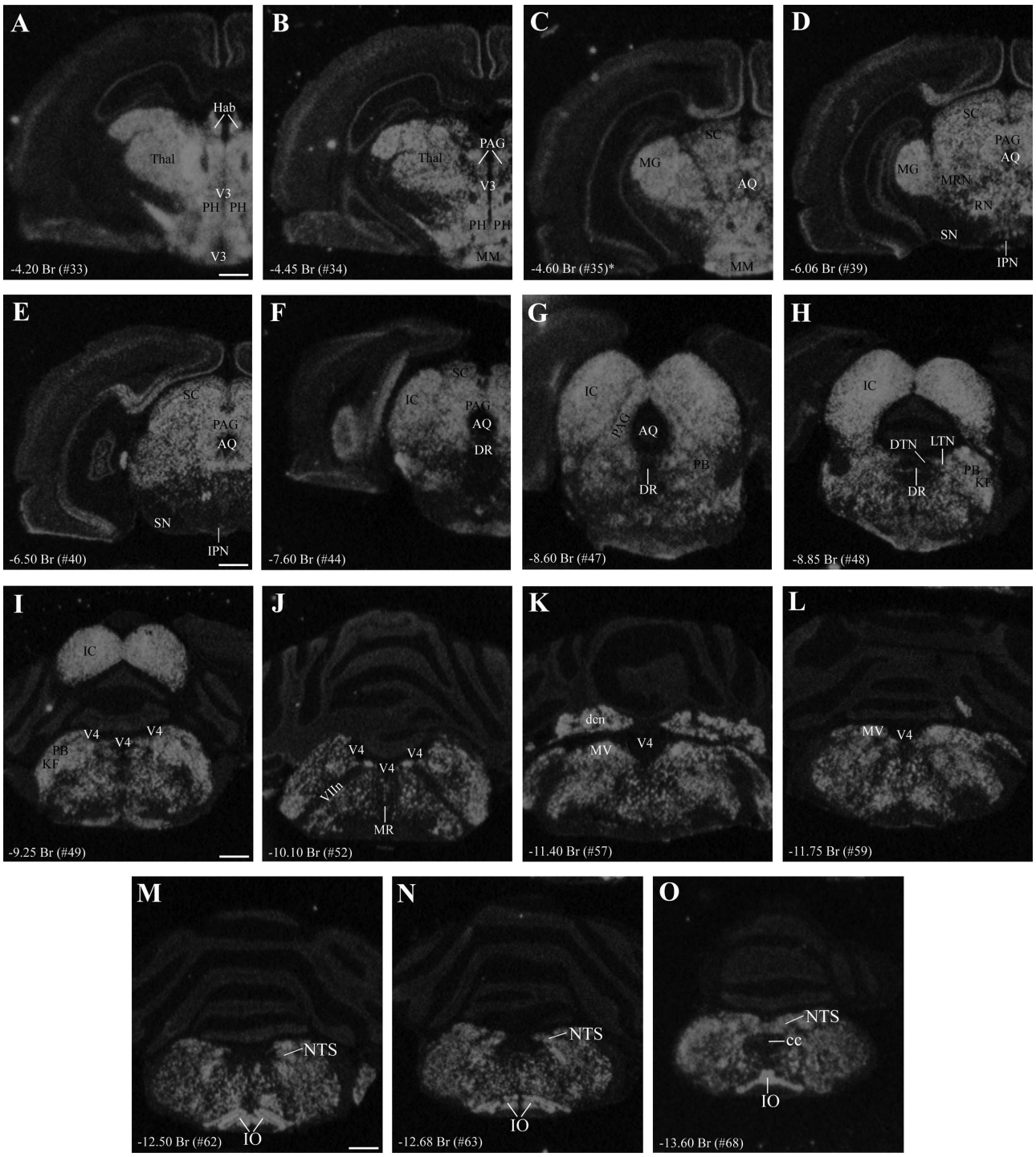

Figure 1. **A–O:** Coronal series presenting gross neuroanatomical distribution of VGLUT2 mRNA in rat brainstem as investigated by single-label *in situ* hybridization. The distribution includes brainstem regions previously identified as PVN-projecting (see text), including the periaqueductal gray (PAG; see B–G), lateral tegmental nucleus (LTN; see H), parabrachial nucleus (PB; see G–I), Kölliker-Fuse subnucleus (KF; see H,I), nucleus of the solitary tract (NTS; see M–O), and ventrolateral region of the medulla containing the A1/C2 cell groups (see M–O). Note robust expression throughout the rostral-caudal extent of PAG (B–G) and relatively low or scattered expression in raphe nuclei (F–J), including dorsal raphe (DR) and raphe magnus (MR). VGLUT2 mRNA expression is present surrounding the LC but not within it (I,J). Additional abbreviations: MRN, mesencephalic reticular nucleus; cc, central canal. For reference, the neuroanatomical level for each panel is indicated by the anterior-posterior distance (millimeters) from bregma (Br) and atlas plate number for the closest matching coronal plate in the brain map of Swanson (2004). Because of differences in plane of section, all structures in any single image might not align exactly with one atlas plate. For example, the asterisk in C indicates that, although hypothalamic anatomy corresponds approximately to plate 35, dorsal regions in this image (AQ, MG, SC) align with more caudal atlas levels. Scale bars = 1 mm. [Color figure can be viewed in the online issue, which is available at wileyonlinelibrary.com.]

sets of sections (i.e., single- vs. double-labeled sections). Sections processed through the combined dual-labeling protocol showed the same cellular pattern of FG immunostaining, although the intensity of the peroxidase reaction product was occasionally lighter in double-labeled material. Regarding VGLUT2 mRNA hybridization signal in dual-labeled vs. hybridization-only sections, the regional variation in VGLUT2 signal also appeared identical, although nonspecific background was higher in the dual-labeled material. Nevertheless, the VGLUT2 signal:background ratio in dual-labeled sections was sufficient to identify VGLUT2-positive or -negative neurons and conformed to previous data on the CNS distribution and regional variation in VGLUT2 expression intensity per section.

VGLUT2 mRNA distribution

A serial presentation of the brainstem distribution of VGLUT2 mRNA is shown is Figure 1, indicating moderate to high expression intensity throughout. The data provide a macroscopic overview of the presence of VGLUT2 in the brainstem, including distribution in brainstem regions previously established as containing PVH-projecting cells: the entire rostral-caudal extent of the periaqueductal gray (Fig. 1B–G), laterodorsal tegmental nucleus (Fig. 1H), lateral and medial parabrachial nuclei (Fig. 1H,I), pedunculopontine nucleus, Kölliker-Fuse nucleus (Fig. 1H,I), nucleus of the solitary tract (Fig. 1M–O), and ventrolateral medulla (encompassing the A1/C1 cell groups), a pattern that is consistent with previous reports (Stornetta et al., 2002; Wang and Morales, 2009). In contrast to most PVH-projecting regions, several raphe nuclei (dorsal, median, magnus) showed sparse signal for VGLUT2 mRNA (Fig. 1E–H).

Retrograde tracing: evaluation and selection of cases

Several cases were collected with confirmation of FG injections of various sizes centered in the PVH, with the extent of the injection sites assessed by FG immunohistochemistry as illustrated schematically in Figure 2A,B. Generally, FG injections were centered at the midrostrocaudal level of the PVH. Cases selected for dual-label data analysis and presentation here were chosen based on 1) rostral-caudal placement, 2) filling of the medial parvocellular portion of the PVH and degree of FG confinement within the PVH boundaries, 3) replication of the forebrain and brainstem distribution of retrograde labeling seen in published studies (Berk and Finkelstein, 1981; Campeau and Watson, 2000; Canteras et al., 1995; Cullinan et al., 1996; Gray et al., 1989; Prewitt and Herman, 1998; Sawchenko et al., 1996, 2000; Swanson, 1987; Swanson and Sawchenko, 1983; Ulrich-Lai et al., 2011), 4) low/sparse FG^+ labeling in the medial or central amygdaloid nuclei (Canteras et al., 1995; Gray et al., 1989; Petrovich et al., 2001; Prewitt and Herman, 1998), and 5) absence of false-positive FG^+ labeling in ventral subiculum, shown by anterograde tracing analysis as supplying a dense innervation immediately outside the PVH borders but not inside (Cullinan et al., 1993). Cases that were excluded from dual-label data analysis, as a result of violation of any of the above-mentioned criteria, are shown in Figure 2B. Thus, the present findings are based primarily on the results for optimal cases (478 shown in Fig. 2A,C; 491 shown in Fig. 2A,D), i.e., placement at the rostrocaudal midlevel of the PVH with spread to the anterior and caudal levels of the PVH but minimal or no detectable spread of FG outside the PVH border; thorough filling of the dorsal parvocellular subdivision; replication of previous findings of retrograde labeling in limbic, preoptic/hypothalamic, thalamic, and brainstem nuclei; sparse (if any) retrograde labeling in amygdaloid nuclei; and absence of FG^+ neurons in ventral subiculum (forebrain data not shown). In contrast, case 495 had an injection centered at a caudal level of the PVH and rostral penetration of tracer only to the midlevel of the PVH, but with substantial spread into the dorsal and caudal peri-PVH region (caudal to the PVH but rostral to the dorsomedial nucleus). Thus, case 495 is included as a comparison that likely reflects localization of FG^+ neurons projecting to the peri-PVN region as well as into the PVH proper (Fig. 2A,E–G).

Retrograde tracing results: brainstem distribution of FG-positive neurons

The distributions of FG-immunopositive neurons in cases 478 and 491 (Figs. 4, 5, respectively) are similar and consistent with previous tract-tracing studies. Highest densities of FG^+ neurons were found in periaqueductal gray (rostral commissural and ventrolateral) and lateral parabrachial nucleus (Figs. 4A–H, 5A–H), with relatively few or scattered neurons in the raphe nuclei (Figs. 4E–H, 5E–H) laterodorsal tegmental area (Figs. 4E–G, 5E–G) and ventrolateral medulla (including the the A1/C1 region; Figs. 4I–L, 5I–L). In addition, a few FG^+ neurons were also present in the Kölliker-Fuse nucleus (Figs. 4I–L, 5I–L), a region that has not been widely reported as a significant source of PVH innervation. In all three cases, relatively few FG^+ neurons were found in the NTS (Figs. 4I–L, 5I–L), but the low numbers observed are commensurate with previous reports typically finding fewer than 10 retrogradely labeled neurons per section (Cunningham et al., 1990; Cunningham and Sawchenko, 1988; Rinaman et al., 1995; Sawchenko et al., 1988; Sawchenko and Swanson, 1981, 1982).

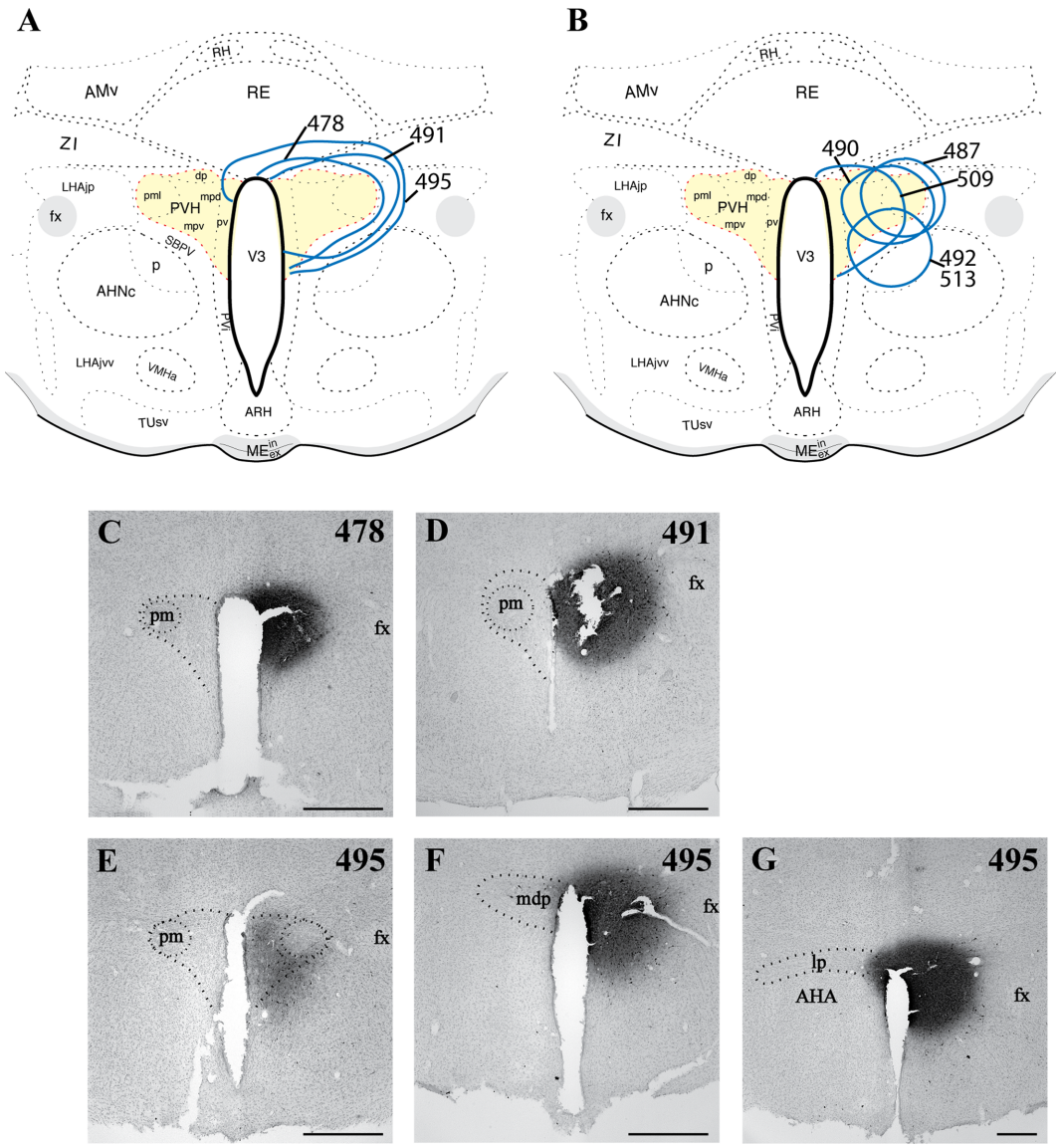

Figure 2. Immunohistochemical and histological assessment of neuroanatomical placement of FG iontophoretic injections in the PVN. **A,B:** Schematic summary of all cases, with most cases centered at the midrostral-caudal level. For each case (rat), the maximal extent of the injection site as assessed by FG chromogenic immunolabeling is denoted by thick solid lines and labeled with a case number. A: Cases for which combined tracing/hybridization results are presented (see Figs. 4–6). B: Cases not presented because of either suboptimal retrograde labeling in brainstem despite effective transport to forebrain afferent regions or slight lateral/ventral misplacement of FG injection. **C:** Case 478, with an injection most prominent at the midrostral-caudal level and nearly limited within the nuclear boundary. **D:** Case 491, placement similar to that of case 478, with minimal spread beyond the nuclear boundary. Note that damage in center of injection site occurred following mounting of free-floating section, as a result of brittleness induced by the peroxidase reaction. **E–G:** Case 495, at three rostral-caudal levels of the PVN. This injection was centered at the caudal end of the PVN (lp, lateral parvocellular subdivision), with significant spread ventrally (F,G), extension caudally into the dorsal area (not shown), and limited detection at the midrostral-caudal level of the PVN (E). Magnification bars = 500 μm (C-F) and 400 μm (G). [Color figure can be viewed in the online issue, which is available at wileyonlinelibrary.com.]

Unlike those in cases 478 and 491, which were centered rostrocaudally at the midlevel of the PVH and were almost entirely circumscribed within the PVH borders, the injection in case 495 was centered at the posterior level of the PVH, i.e., in the lateral (aka posterior) parvocellular subdivision, with a maximal extent reaching rostrally to the midlevel of PVH and caudally into the dorsal area (the internuclear between the caudal end of the PVH and the rostral border of the dorsomedial hypothalamic nucleus; Fig. 2A,C–E). Thus, the results for case 495 are presented in Figure 6 as a comparison case for the well-circumscribed FG placements in the others. Case 495 differed from cases 478 and 491 in both a quantitative and a regional manner, with greater numbers of FG^+

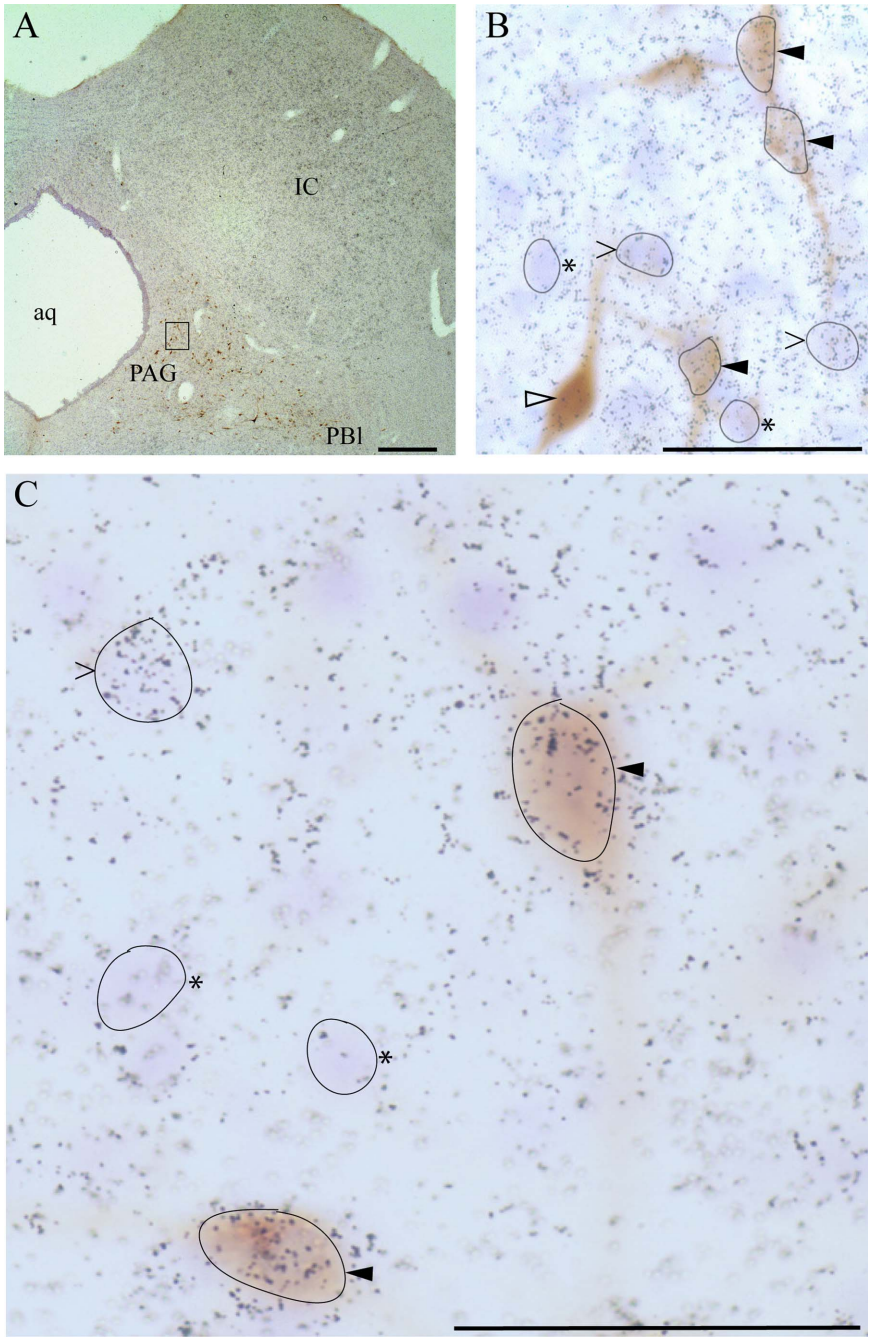

Figure 3. Example of combined FG immunolabeling (chromogenic, brown DAB product) and ^{35}S-labeled riboprobe detection (grain clustering) of VGLUT2 mRNA from emulsion-dipped slide. **A:** Low-magnification view of section through periaqueductal gray (PAG). Note that dipped sections were lightly counterstained with cresyl violet. FG-positive neurons can be seen within the ventrolateral PAG and extending laterally toward the parabrachial nucleus (PB). Box denotes region shown at higher magnification in B. **B:** Micrographs providing examples of dual-labeled FG$^+$/VGLUT2$^+$ neurons (solid arrowheads), FG$^+$ only (open arrowhead), and FG-negative VGLUT2$^+$ neurons (> symbols), as determined from grain counts over Nissl-stained cell body (see Materials and Methods). Examples of neurons negative for both FG and VGLUT2 (Nissl-positive) are denoted by asterisks. Note: some neurons have been outlined in black to correspond to somatic contours from the optimal focal plane. **C:** Higher magnification view (×100, oil immersion) of a FG/VGLUT2 dual-labeled neuron as well as VGLUT2-only and Nissl-only neurons. Scale bars = 400 μm in A; 50 μm in B,C.

neurons in most regions where retrograde labeling was seen in cases 478 and 491. However, case 495 produced FG$^+$ neurons in brainstem regions not labeled in cases 478 and 491: medial parabrachial nucleus (Fig. 6E,F), pedunculopontine nucleus (Fig. 6E,F), and nucleus raphe magnus (RM; Fig. 6G,H), which likely reflected

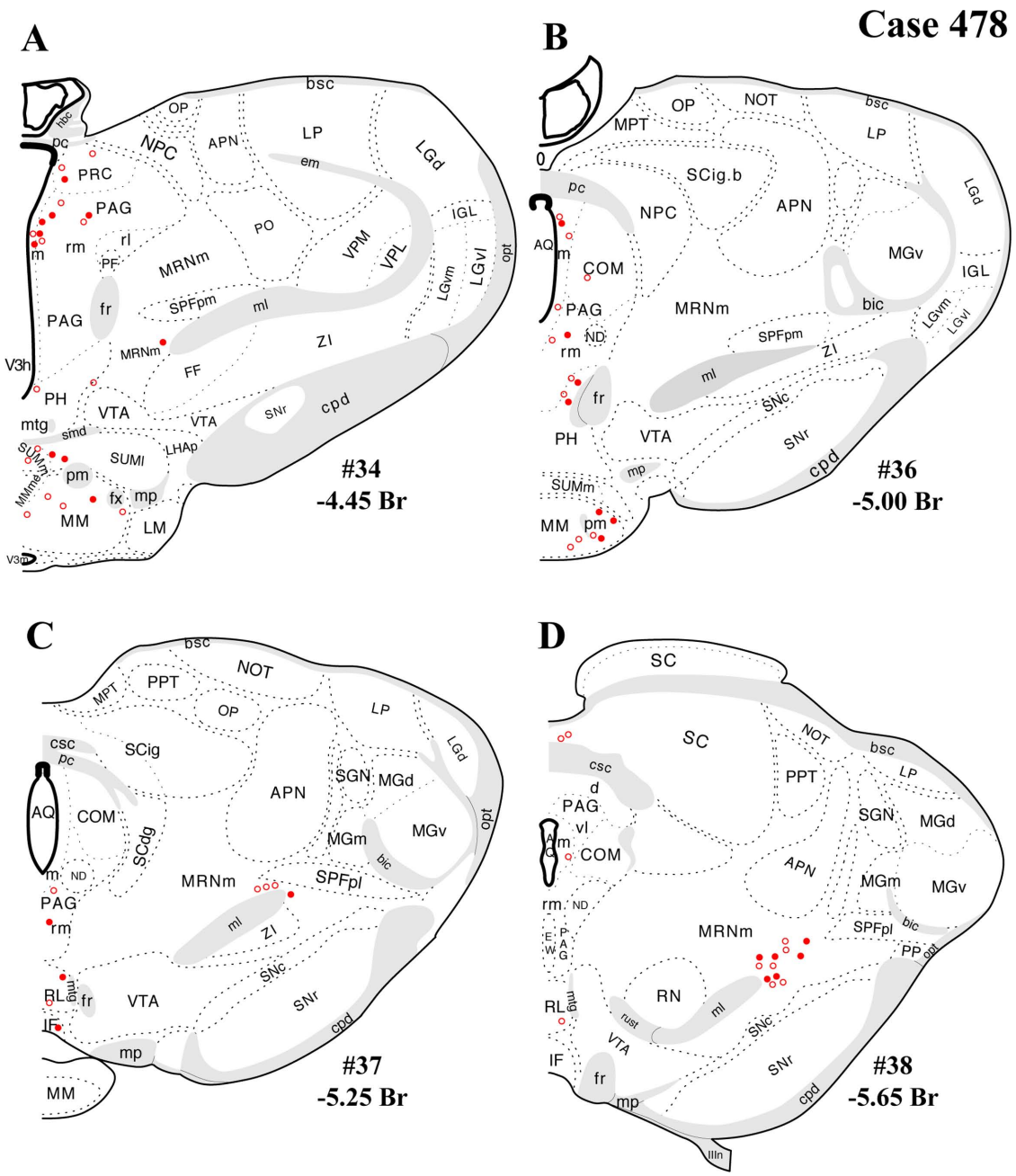

Figure 4. A–L: Case 478 results. Schematic coronal map of FG^+ neurons either dually labeled for VGLUT2 mRNA (solid circles) or negative for VGLUT2 (open circles). Each coronal template is derived from the rat brain atlas of Swanson (2004) and denoted with the plate number (34-69) and rostral-caudal coordinate relative to bregma (in millimeters). For regional VGLUT2 mRNA expression, compare with Figure 1 and see Results. [Color figure can be viewed in the online issue, which is available at wileyonlinelibrary.com.]

uptake from the caudal PVH or from the region caudal to the nucleus itself.

Dual-labeled FG^+/$VGLUT2^+$ neurons

After the dual-labeling procedures, sections from each of the three cases presented were analyzed, and the location of each FG^+ neuron was plotted on a coronal template diagram. The coronal maps of FG labeling and dual labeling in cases 478, 491, and 495 (Figs. 4–6) represent 12 rostral-caudal levels chosen from the entire sequence of brainstem sections based on 1) highest level of FG^+ or dual FG^+/$VGLUT2^+$ labeling and 2) levels in which the closest anatomical matching across cases could be achieved.

In general, all brainstem regions that contained retrogradely labeled (FG^+) neurons also displayed dual FG^+/$VGLUT2^+$ labeling. As can be seen in Figures 4 and 5 (cases 478 and 491), the regions with the most

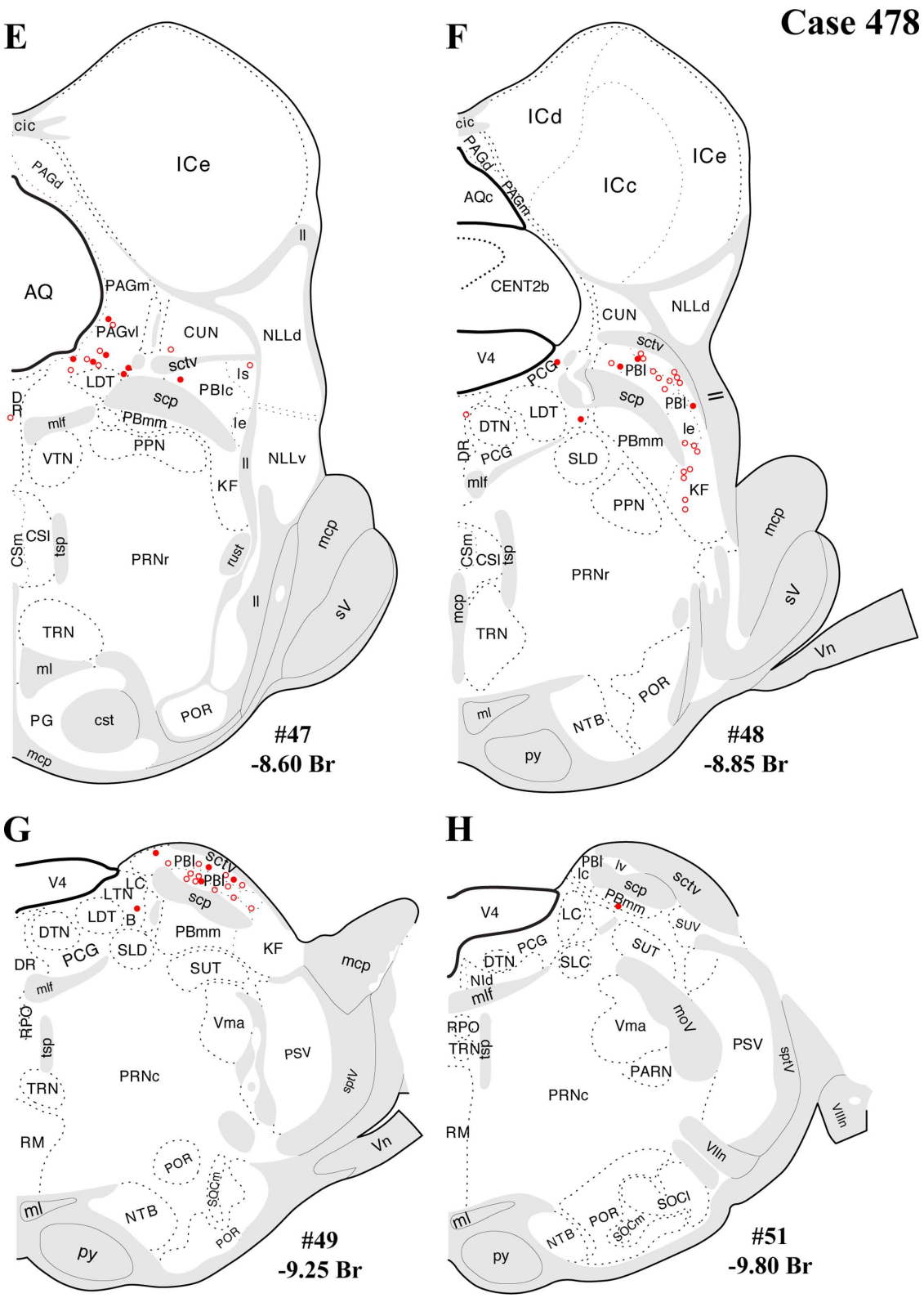

Figure 4. (Continued)

substantial FG^+/$VGLUT2^+$ dual labeling were the periaqueductal gray (Figs. 4A–F, 5A–F), the lateral parabrachial nucleus, and the Kölliker-Fuse subnucleus (Figs. 4E–H, 5E–H). A quantitative assessment of the total number FG^+ neurons per region and dual labeling (as a percentage of total number FG^+ neurons) is reported in

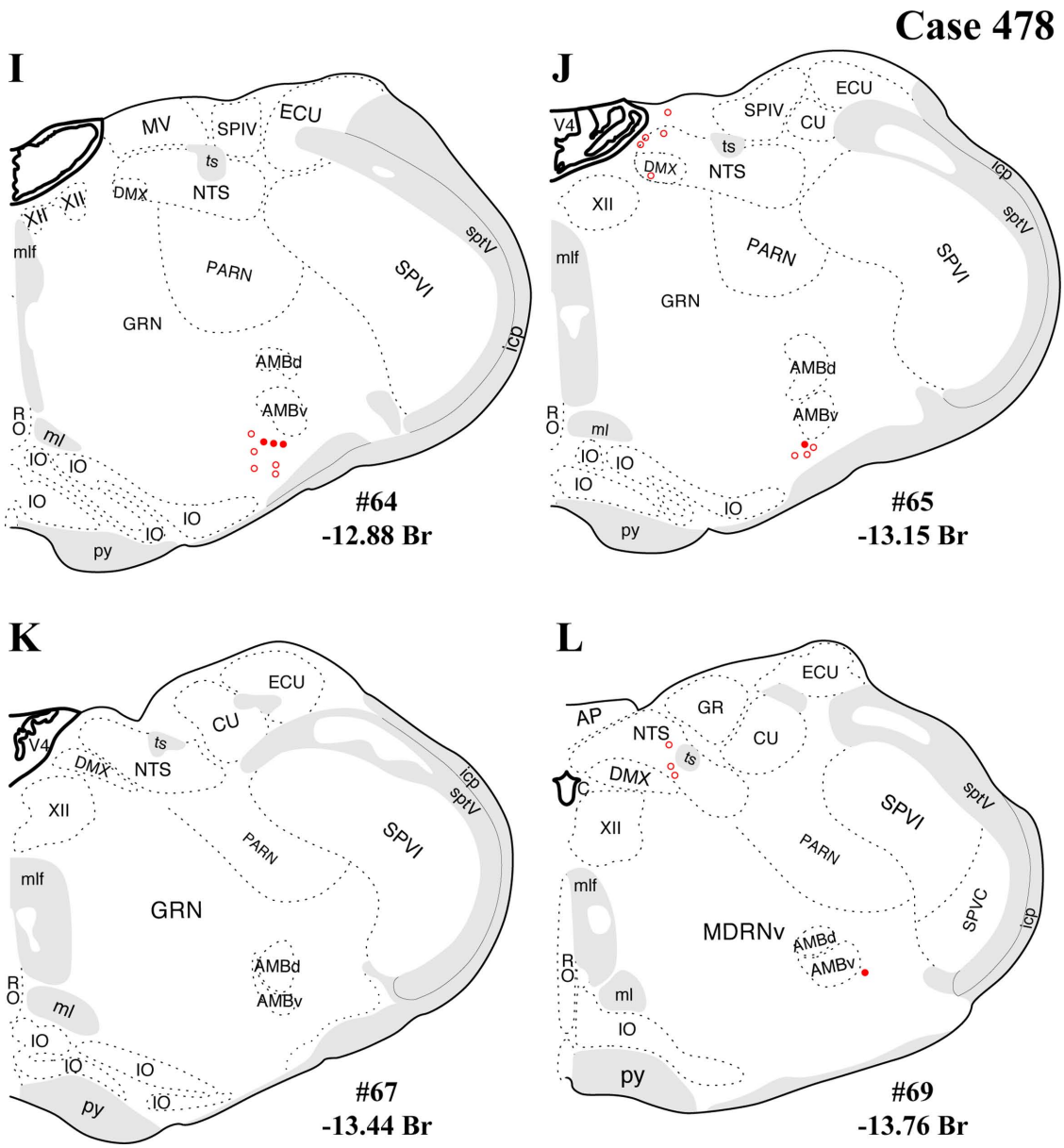

Figure 4. (Continued)

Table 1. These tabulated data reflect a summation from all sections analyzed through each region. As noted in Materials and Methods, the true total numbers of single-labeled FG^+ neurons or dual-labeled neurons per brain regions is probably greater than sixfold times the neuron numbers listed in Table 1. Experimental factors preclude providing an exact, quantitative extrapolation from neuron numbers in Table 1 to the true totals per brain region.

In addition, substantial numbers FG^+ and dual-labeled neurons were also found in a midbrain area surrounding the dorsolateral portion of the medial lemniscus, straddling a territory belonging to the mesencephalic reticular nucleus ("MRNm"), and the caudal portion of the zona incerta (Figs. 4B–D, 5B–D). Brain regions containing FG^+ neurons that showed a very low proportion of dual-labeled neurons included the ventrolateral medulla (ventral or ventromedial to the nucleus ambiguous; Figs. 4I–L, 5I–L), which includes neurons of the A1/C1 cell groups known to project to the PVH (Stornetta et al., 2002).

Note that the illustrations of single FG^+ labeling and dual labeling within the periaqueductal gray mostly highlights rostral and caudal levels where most retrograde labeling was found, in line with previous studies (see Discussion). Levels between those shown in each coronal series were not included because of comparatively sparse FG^+ labeling and imprecise anatomical matching of

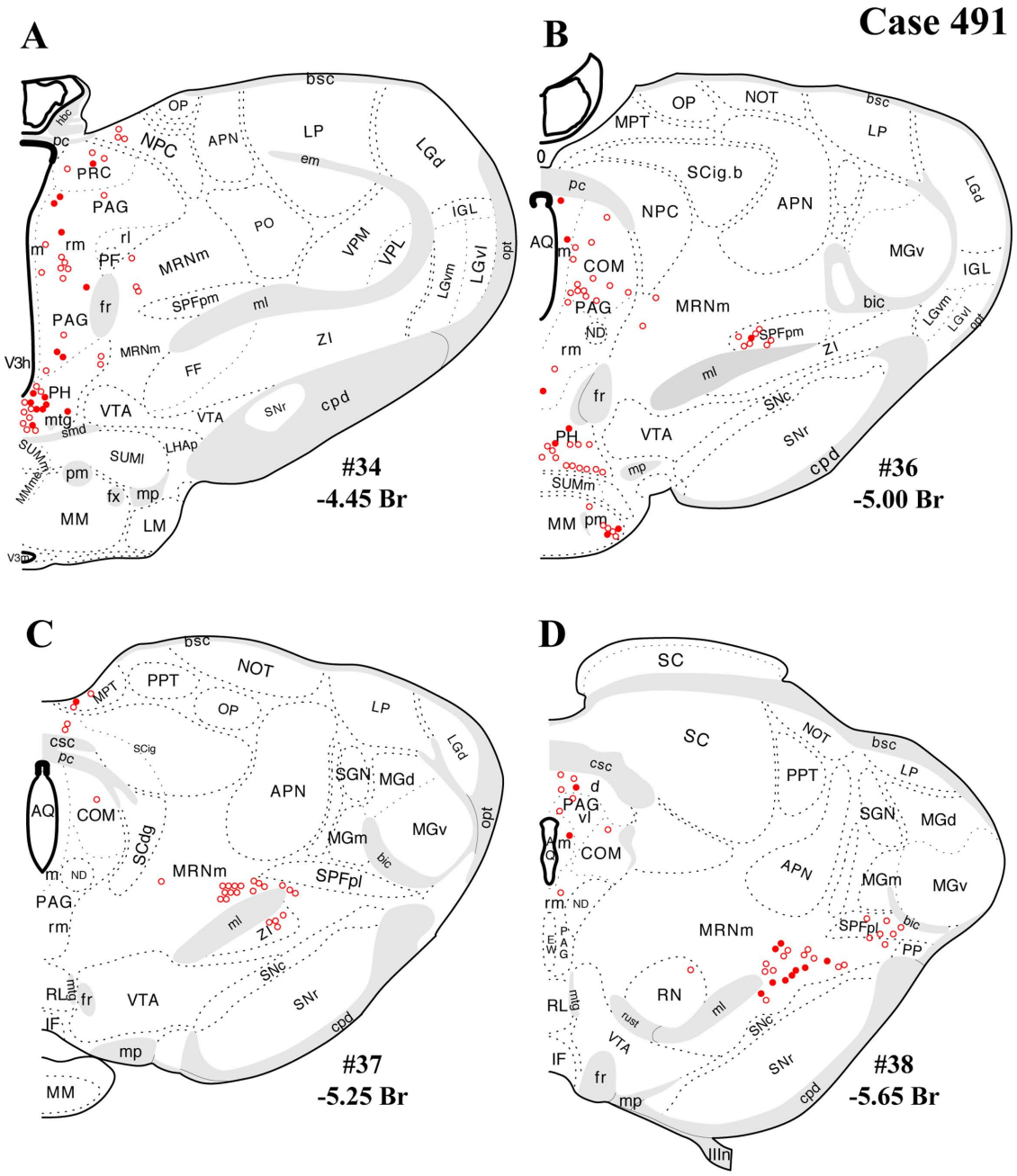

Figure 5. A–L: Case 491 results. Schematic coronal map of FG^+ neurons either dually labeled for VGLUT2 mRNA (solid circles) or negative for VGLUT2 (open circles). Each coronal template is derived from the rat brain atlas of Swanson (2004) and denoted with the plate number (34-69) and rostral-caudal coordinate relative to bregma (in millimeters). For regional VGLUT2 mRNA expression, compare with Figurde 1 and see Results. [Color figure can be viewed in the online issue, which is available at wileyonlinelibrary.com.]

sections between cases 478 and 491. In case 491, for example, at rostral-caudal levels between those shown in the figures, the dorsomedial "column" showed 0–10 FG^+ neurons per section, with fewer neurons seen in the other columns at the same levels (dorsolateral, lateral, ventrolateral).

The present distribution of dual-labeled neurons is also consistent with the observed regional variation in VGLUT2 mRNA expression shown in Figure 1. Specifically, robust VGLUT2 mRNA is seen throughout the rostral-caudal range of the periaqueductal gray (Fig. 1B–G), including the rostral level of periaqueductal gray (precommissural nucleus, rostromedial and medial subdivisions, commissural nucleus), where FG^+/$VGLUT2^+$ neurons were found (Figs. 1B,C 4A–D, 5A–D, 6A–D), and the caudal level of the ventrolateral column (Figs. 1G, 4E,F, 5EF, 6E,F). A similar relationship was found dual labeling in the lateral parabrachial nucleus (Figs. 4E–G, 5E–G, 6E–G, with

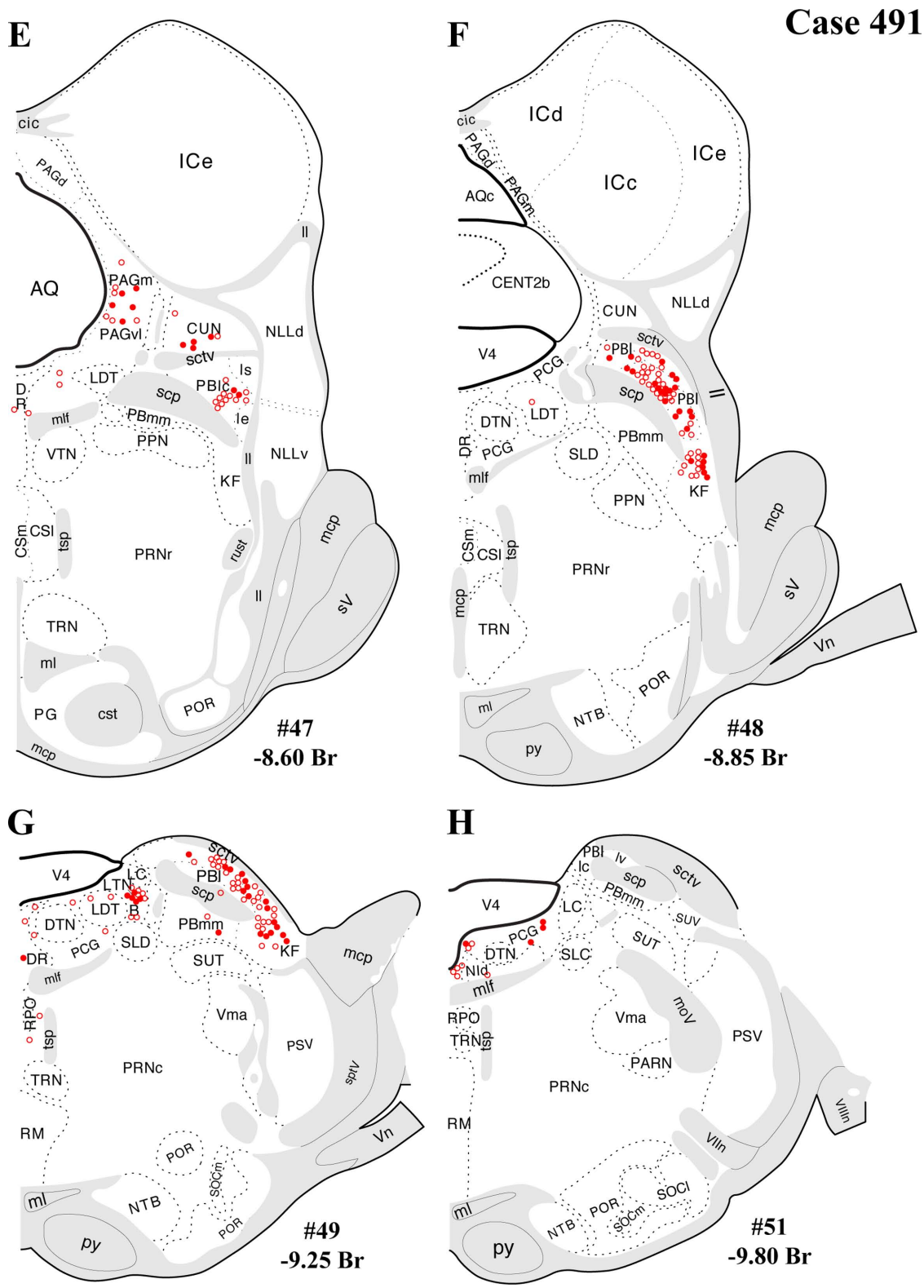

Figure 5. (Continued)

VGLUT2 mRNA expression shown in Fig. 1G–I). In contrast, for example, the lack of substantial dual labeling in the dorsal or magnus raphe nuclei (Figs. 4E–H, 5E–H, 6E–H) is not surprising given the low to undetectable VGLUT2 mRNA signal in these midline regions (Fig. 1F–H) as well the sparse presence of FG^{+} neurons (in our cases).

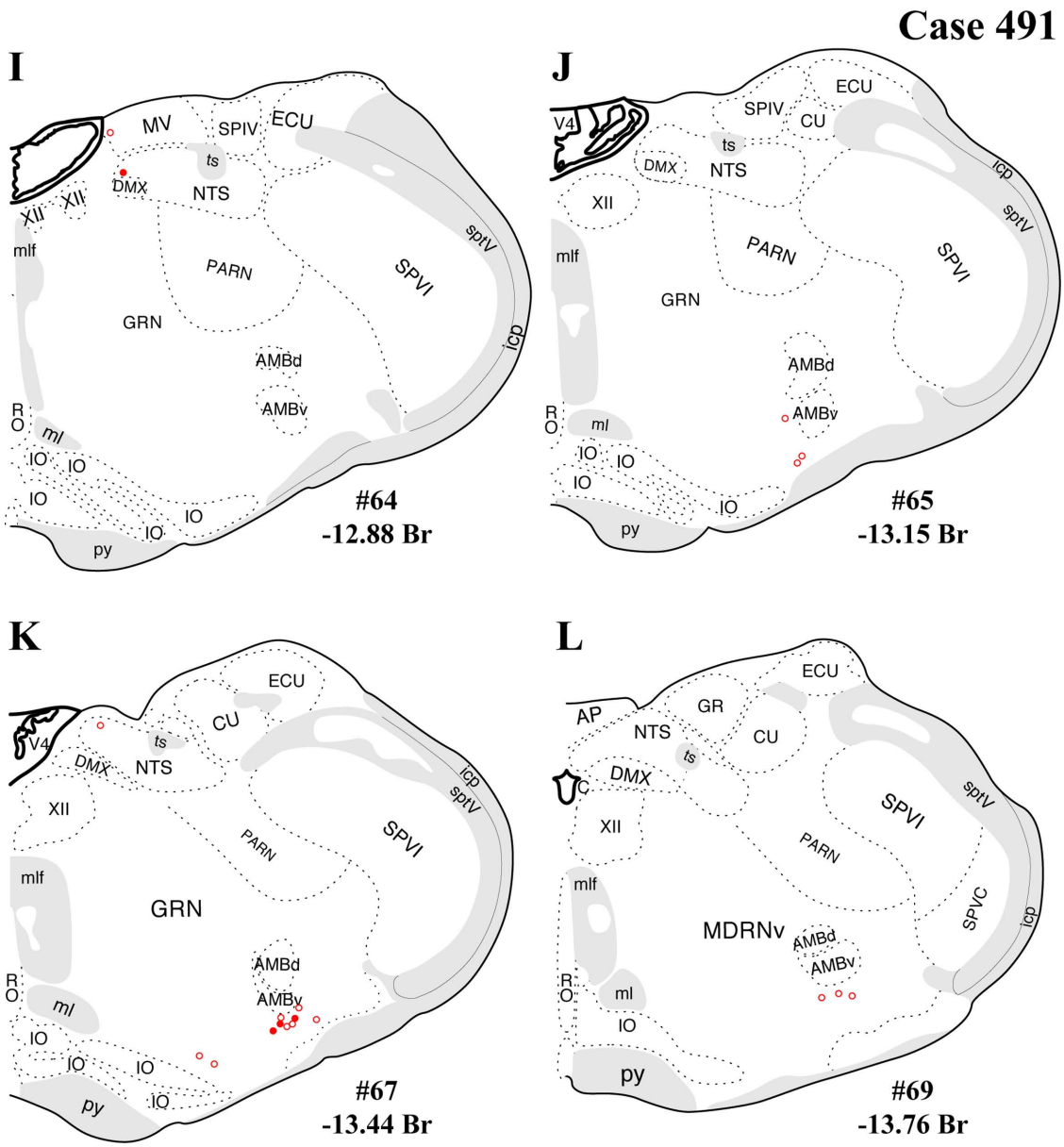

Figure 5. (Continued)

DISCUSSION

Summary of dual-labeling findings

The brainstem regions with the most significant numbers of $FG^+/VGLUT2^+$ dual-labeled neurons (derived from cases 478 and 491; those with well circumscribed FG injections in the PVH) were the periaqueductal gray, lateral parabrachial nucleus, and a caudal thalamic/midbrain reticular area. The present cases displayed only modest retrograde labeling (per section) in the nucleus of the solitary tract (A2) and ventrolateral medulla (A1), precluding meaningful assessment of potential FG/VGLUT2 dual labeling in these regions. In case 495, an FG injection centered in the caudal PVH with significant spread into the peri-PVH region ventrally (subparaventricular zone) and caudally displayed FG^+ labeling in three additional regions where cases 478 and 491 lacked FG^+ neuronal labeling, the medial parabrachial nucleus, pedunculopontine nucleus, and median raphe nucleus, and included some $FG^+/VGLUT2^+$ neuronal labeling in these areas as well. The presence of $FG^+/VGLUT2^+$ neurons in these three additional brainstem regions is likely evidence for glutamatergic innervation to the peri-PVH region, rather than the PVH itself.

Functional implications and context of dual-labeling findings

The present identification of the major brainstem sources of glutamatergic innervation (periqueductal gray,

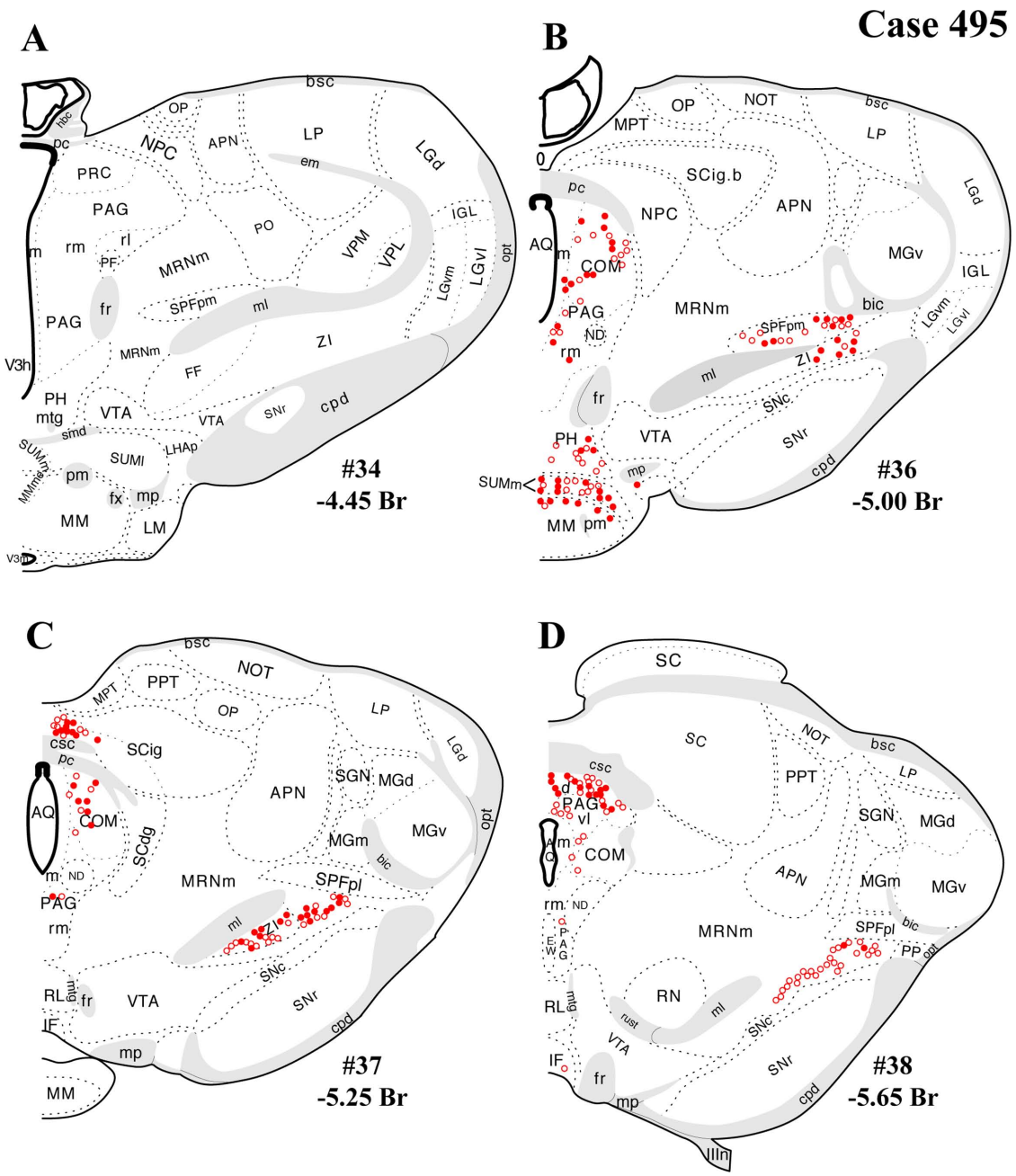

Figure 6. A–L: Case 495 results. Schematic, coronal map of FG^+ neurons either dually labeled for VGLUT2 mRNA (solid circles) or negative for VGLUT2 (open circles). Each coronal template is derived from the rat brain atlas of Swanson (2004) and denoted with the plate number (34-69) and rostral-caudal coordinate relative to bregma (in millimeters). For regional VGLUT2 mRNA expression, compare with Figure 1 and see Results. [Color figure can be viewed in the online issue, which is available at wileyonlinelibrary.com.]

lateral parabrachial nucleus, caudal thalamus/mesencephalic reticulum). significantly extends prior understanding of ascending HPA-excitatory neural pathways. Although noradrenergic/adrenergic and serotonergic projections to the PVH have garnered most of the attention to date regarding brainstem input to the PVH, the present findings serve to highlight additional sources of excitatory input to the PVH, including a region largely ignored thus far by functional studies of HPA-regulatory neurocircuitry (rostral PAG and caudal ventrolateral PAG). A full appreciation of the significance of these brainstem sites requires integrating the current data with the prior state of knowledge about these regions.

Periaqueductal gray

The periaqueductal gray is a known PVH-projecting structure in which substantial proportions of FG^+/$VGLUT2^+$ neurons were detected. Previous retrograde

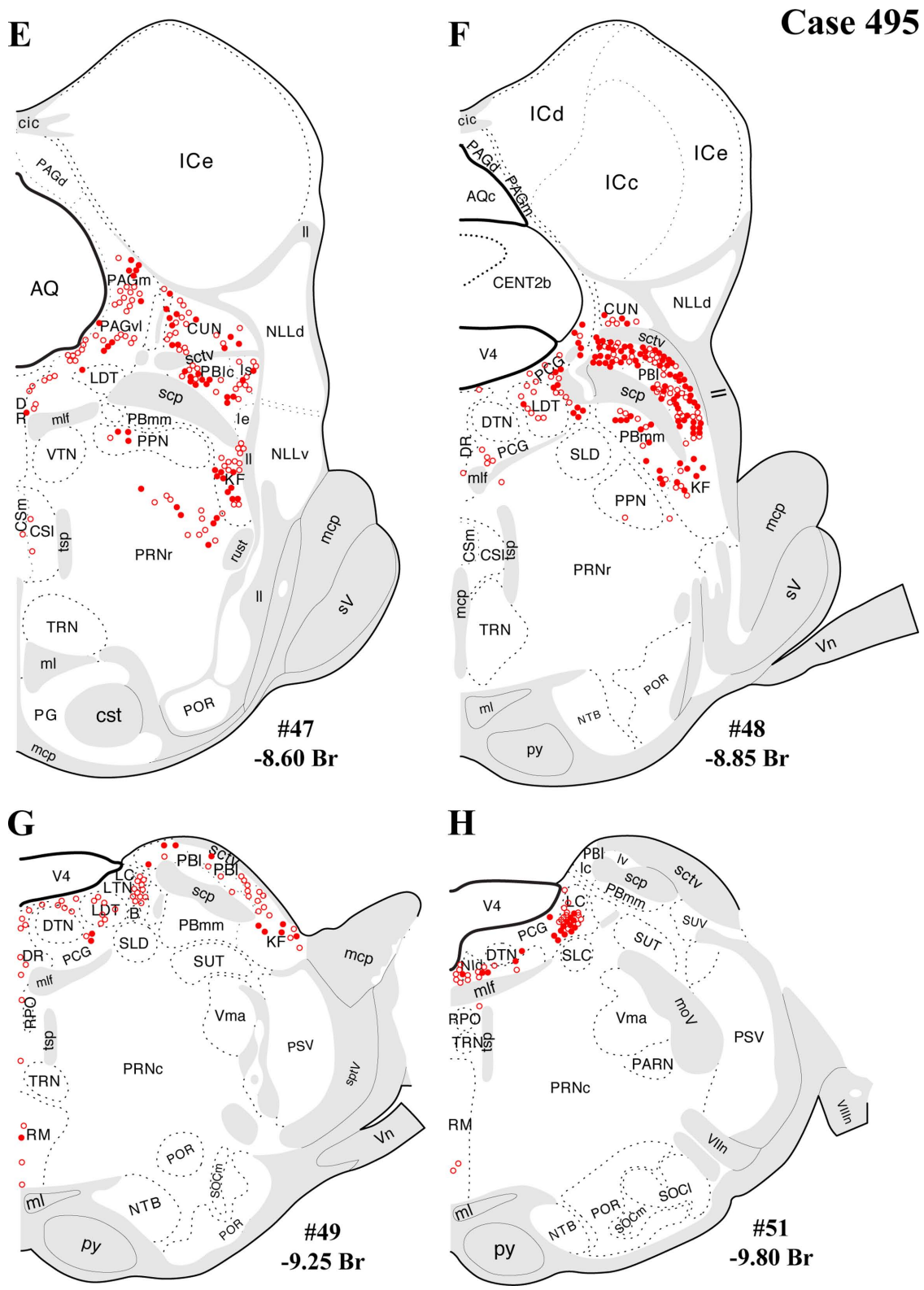

Figure 6. (Continued)

and anterograde tracing studies have documented PAG projections to the PVH originating mainly from the pre-commissural and commissural subdivisions, dorsolateral column, and ventrolateral column (Berk and Finkelstein, 1981; Cameron et al., 1995; Floyd et al., 1996; Krout and Loewy, 2000; Sawchenko and Swanson, 1983). The

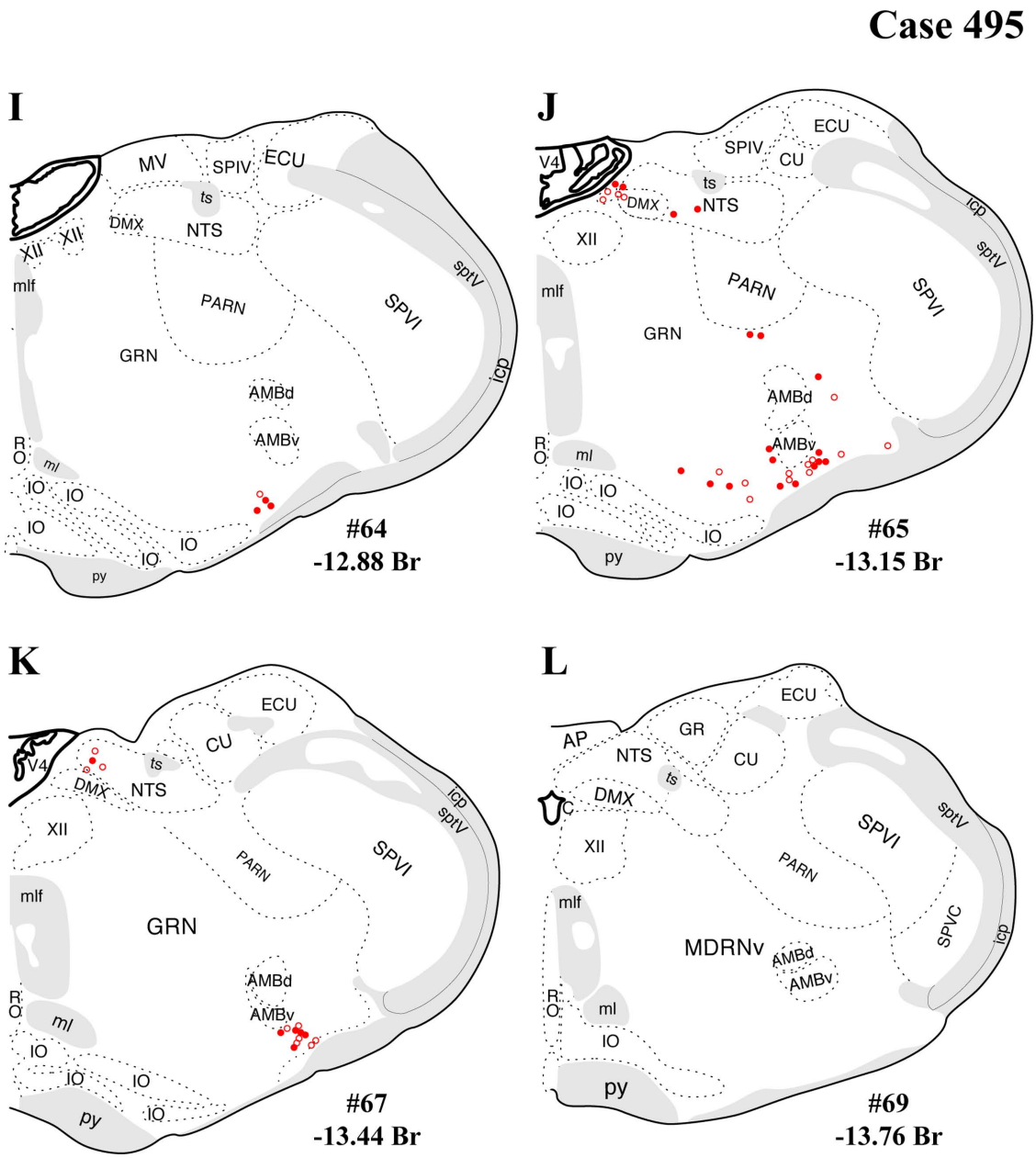

Figure 6. (Continued)

present data included dual-labeled neurons in the rostral subdivisions at the level of the posterior commissure and at a caudal level of the ventrolateral column. A similar density of FG^+ (single-labeled) and $FG^+/VGLUT2^+$ neurons were also present at more rostral levels of the ventrolateral and dorsolateral columns of the PAG, although these levels were not included in the figures because of imprecise anatomical matching of sections across different cases.

The present evidence for glutamatergic PVH-projecting neurons in rostral subdivisions (precommissural, rostromedial, medial, and commissural) and the caudal ventrolateral subdivision of the PAG takes on new functional significance when integrated with previous studies of stress-induced CNS activation analyses (immediate early gene activation), microinjection/lesion studies of PAG function, and convergence of afferent input to the PAG from upstream stress-related regions.

First, with regard to the rostral subdivisions, the present data are consistent with previous anterograde tracing findings of substantial PVH innervation from the precommissural nucleus and rostromedial region (Canteras and Goto, 1999; Krout and Loewy, 2000). These rostral sites also show IEG responses to a subset of acute stressors

tested to date: robust c-fos mRNA or Fos responses to elevated plus maze, predator stress, and acute defeat (conspecific; Canteras and Goto, 1999; Kollack-Walker et al., 1999; Silveira et al., 1993) but weak c-fos mRNA responses to loud noise, swim, or restraint (Campeau and Watson, 1997; Cullinan et al., 1995). Furthermore, this site receives input from upstream regions known to regulate HPA function, including medial prefrontal cortex, lateral septum, and hypothalamic nuclei (Bandler and Shipley, 1994; Canteras and Goto, 1999). Intriguingly, although the rostral level of the PAG has received little attention in published mechanistic studies of the role of the PAG in regulating anxiety/stress-related behavior, fear learning, or HPA function, this rostral PAG region receives significant projections from the dorsomedial, dorsolateral, and lateral PAG columns (Canteras and Goto, 1999), all of which lack substantial projections to the PVH (Krout and Loewy, 2000) but have nonetheless been implicated in regulating HPA and autonomic function. Specifically, panic/escape-inducing electrical stimulation of the dorsolateral column also induces a corticosterone response (Lim et al., 2011), whereas muscimol inhibition of the dorsolateral/lateral columns attenuates the ACTH response to air-jet stress (de Menezes et al., 2008). In addition, local stimulation of the dorsolateral PAG with NMDA increases blood pressure, an effect that is blocked by NMDA receptor blockade within the PVH (Berrino et al., 1996). Thus, given the evidence against substantial projections from these three columns to the PVH collectively, the present date raise the possibility of an indirect neuroanatomical pathway, whereby dorsal and lateral PAG columns activate the neuroendocrine and preautonomic components of the PVH ultimately via glutamatergic projection from the rostral PAG.

The caudal ventrolateral PAG, a second major subdivision in which dual labeling was found, has received comparatively more attention. Previous anterograde studies have documented that this subdivision supplies a dense innervation of the PVH, in contrast to most other PAG subdivisions (Canteras and Goto, 1999; Krout and Loewy, 2000). The ventrolateral column also shows strong neuronal activation to a broad range of acute stressors, including physiological challenges (e.g., hypovolemia), painful or noxious stimuli (e.g., cutaneous/muscular/visceral pain, foot shock), cold exposure, swim stress, and external threats (e.g., dominant conspecific; Bellchambers et al., 1998; Canteras and Goto, 1999; Cullinan et al., 1995; Keay and Bandler, 1993; Keay et al., 2000, 2001; Li and Sawchenko, 1998; Motta et al., 2009; Vagg et al., 2008; Yoshida et al., 2005). Notably, the degree of stress-induced activation in the ventrolateral PAG varies across stimuli, and other PAG subdivisions are more sensitive than ventrolateral PAG to specific stressors, e.g., predator odor/presence (Canteras and Goto, 1999; Motta et al., 2009). Thus, the evidence suggests that glutamatergic input to the PVH from ventrolateral PAG likely is involved in transducing a range of physiological as well as psychogenic stressors. Furthermore, the ventrolateral PAG receives an array of input from both HPA-excitatory and -inhibitory regions, including ascending visceral and somatic sensory input from the NST and spinal nociceptive projections, as well as descending input from orbitofrontal, insular, and medial prefrontal cortex; central amygdaloid nucleus; and several hypothalamic nuclei (Bandler and Shipley, 1994; Keay and Bandler, 2004). Furthermore, microinjection of the opiate analgesic buprenorphine into the caudal ventrolateral PAG suppresses plasma ACTH and corticosterone (Gomez-Flores and Weber, 2000), which would be consistent with inhibition of a site supplying glutamatergic projections to the PVH. Thus, glutamatergic projections from the caudal ventrolateral PAG to the PVH may serve as a critical point of integration for multiple HPA-regulatory brain regions encoding multiple types of stress, especially for upstream regions that lack substantial direct projections to the PVH (e.g., orbital and medial prefrontal cortex).

Lateral parabrachial nucleus

Another major source of brainstem glutamatergic input to the PVH indicated by the present data is the lateral parabrachial nucleus (PBl). This finding extends the existing literature documenting PBl projections to the PVH (Alden et al., 1994; Bester et al., 1997; Krukoff et al., 1993), neuronal activation of the PBN by various stressors, and functional evidence for a HPA-excitatory role for the PBN. Specifically, previous studies show induction of c-fos or other IEGs in the parabrachial nucleus after a range of stressors, including restraint, foot shock, hemorrhage, inflammatory cytokine challenge (IL-1β), and lithium chloride (nauseant) administration (Chan and Sawchenko, 1994; Kainu et al., 1993; Li and Sawchenko, 1998; Sawchenko et al., 1996; Spencer and Houpt, 2001; St. Andre et al., 2007). This profile of stress responsiveness of the PBN, including the lateral PBN, is consistent with its afferent input from other brainstem or spinal cord regions that relay respiratory, cardiovascular, visceral sensory, and nociceptive information, i.e., from deep laminae and lamina I of the dorsal horn, NST, pre-Botzinger nucleus, and dorsal/ventral respiratory groups (Ezure, 2004; Gauriau and Bernard, 2002). In addition, chemical stimulation of lateral parabrachial neurons in anesthetized animals induces ACTH secretion (Carlson et al., 1994). Thus, the present data point to the glutamatergic PBl projections to the PVH as a possible neuroanatomical mechanism for stress-induced HPA activation, particularly by respiratory and hemodynamic stimuli, LiCl, and

foot shock. Furthermore, beyond mediating HPA activation by such unconditioned stimuli, the medial and lateral parabrachial nuclei have also been implicated in LiCl-mediated conditioned taste aversion (CTA; Reilly, 1999; Reilly and Trifunovic, 2001). This form of associative learning is enhanced by the LiCl-induced glucocorticoid response and impaired by experimental attenuation of this LiCl-induced HPA response (Smotherman et al., 1976). Thus, our evidence for glutamatergic innervation of the PVH from the PBl provides a possible mechanistic basis for glucocorticoid-mediated enhancement of aversive learning.

Caudal thalamus/midbrain reticulum

Another locus of $FG^+/VGLUT2^+$ dual labeling was found at a caudal level of the thalamus and zona incerta surrounding the medial lemniscus, spanning a dorsolateral portion of caudal zona incerta, mesencephalic reticular area, and a part of the subparafascicular nucleus of the thalamus (see Results; Figs. 4, 5), consistent with an earlier retrograde labeling study (Berk and Finkelstein, 1981). Evidence for connectivity between the zona incerta and PVH has thus far been restricted to a rostral and ventromedial portion of the zona incerta and suggested to supply dopaminergic input to the PVH (Cheung et al., 1998; Wagner et al., 1995). The present data suggest a role for glutamate in this projection. Moreover, the present evidence for dual-labeled neurons within the subparafascicular nucleus is consistent with a previous study implicating the region in responsiveness to audiogenic stress (Campeau and Watson, 2000), a stressor known to activate both PVH neurons and the HPA axis (Burow et al., 2005; Campeau and Watson, 1997, 2000; Helfferich and Palkovits, 2003; Michaud et al., 2003; Palkovits et al., 2004). Thus, the present findings support the possibility that audiogenic stress activates the PVH and HPA axis via glutamatergic PVH projections.

SUMMARY

The present findings indicate that several brainstem regions, particularly the periaqueductal gray and lateral parabrachial nucleus, are brainstem origins of glutamatergic projections to the PVH. In addition, a third source of glutamatergic input emanates from a diencephalic/mesencephalic area, encompassing a caudal portion of the zona incerta, the mesencephalic reticular nucleus, and the subparafascicular nucleus of the thalamus. These observations, made in cases with well-circumscribed retrograde tracer injections into the PVH, are consistent with previous tracing studies as well as with previous and present reports on the CNS distribution of VGLUT2 mRNA expression. The present data implicate the periaqueductal gray and lateral parabrachial nucleus as HPA-excitatory regions that activate neuroendocrine stress responses via glutamatergic activation of the PVH. Judged from previous studies of the functions of these regions and their responses to a range of stressful stimuli, these ascending glutamatergic inputs to the PVH are potentially involved in regulating HPA responses to multiple classes of stress (physiological/interoceptive, or psychological/exteroceptive, or mixed) and, moreover, may serve as points of stress integration proximal to the PVH. This ascending glutamatergic input is also likely integrated at the level of the PVH with glutamatergic innervation originating from forebrain origins, which have recently been elucidated (Ulrich-Lai et al., 2011).

LITERATURE CITED

Aihara Y, Mashima H, Onda H, Hisano S, Kasuya H, Hori T, Yamada S, Tomura H, Yamada Y, Inoue I, Kojima I, Takeda J. 2000. Molecular cloning of a novel brain-type Na^+-dependent inorganic phosphate cotransporter. J Neurochem 74:2622–2625.

Al-Ghoul WM, Meeker RB, Greenwood RS. 1997. Differential expression of five N-methyl-D-aspartate receptor subunit mRNAs in vasopressin and oxytocin neuroendocrine cells. Brain Res 44:262–272.

Alden M, Besson JM, Bernard JF. 1994. Organization of the efferent projections from the pontine parabrachial area to the bed nucleus of the stria terminalis and neighboring regions: a PHA-L study in the rat. J Comp Neurol 341: 289–314.

Antoni FA. 1986. Hypothalamic control of adrenocorticotropin secretion: advances since the discovery of 41-residue corticotropin-releasing factor. Endocr Rev 7:351–378.

Aubry JM, Bartanusz V, Pagliusi S, Schulz P, Kiss JZ. 1996. Expression of ionotropic glutamate receptor subunit mRNAs by paraventricular corticotropin-releasing factor (CRF) neurons. Neurosci Lett 205:95–98.

Bai L, Xu H, Collins JF, Ghishan FK. 2001. Molecular and functional analysis of a novel neuronal vesicular glutamate transporter. J Biol Chem 276:36764–36769.

Bandler R, Shipley MT. 1994. Columnar organization in the midbrain periaqueductal gray: modules for emotional expression? Trends Neurosci 17:379–389.

Barroso-Chinea P, Castle M, Aymerich MS, Perez-Manso M, Erro E, Tunon T, Lanciego JL. 2007. Expression of the mRNAs encoding for the vesicular glutamate transporters 1 and 2 in the rat thalamus. J Comp Neurol 501: 703–715.

Bartanusz V, Muller D, Gaillard RC, Streit P, Vutskits L, Kiss JZ. 2004. Local gamma-aminobutyric acid and glutamate circuit control of hypophyseotrophic corticotropin-releasing factor neuron activity in the paraventricular nucleus of the hypothalamus. Eur J Neurosci 19:777–782.

Bellchambers CE, Chieng B, Keay KA, Christie MJ. 1998. Swim-stress but not opioid withdrawal increases expression of c-fos immunoreactivity in rat periaqueductal gray neurons which project to the rostral ventromedial medulla. Neuroscience 83:517–524.

Bellocchio EE, Hu H, Pohorille A, Chan J, Pickel VM, Edwards RH. 1998. The localization of the brain-specific inorganic phosphate transporter suggests a specific presynaptic role in glutamatergic transmission. J Neurosci 18: 8648–8659.

Bellocchio EE, Reimer RJ, Fremeau RT Jr, Edwards RH. 2000. Uptake of glutamate into synaptic vesicles by an inorganic phosphate transporter. Science 289:957–960.

Berk ML, Finkelstein JA. 1981. Afferent projections to the preoptic area and hypothalamic regions in the rat brain. Neuroscience 6:1601–1624.

Berrino L, Pizzirusso A, Maione S, Vitagliano S, D'Amico M, Rossi F. 1996. Hypothalamic paraventricular nucleus involvement in the pressor response to N-methyl-D-aspartic acid in the periaqueductal grey matter. Naunyn-Schmiedebergs Arch Pharmacol 353:157–160.

Bester H, Besson JM, Bernard JF. 1997. Organization of efferent projections from the parabrachial area to the hypothalamus: a *Phaseolus vulgaris*-leucoagglutinin study in the rat. J Comp Neurol 383:245–281.

Boudaba C, Schrader LA, Tasker JG. 1997. Physiological evidence for local excitatory synaptic circuits in the rat hypothalamus. J Neurophysiol 77:3396–3400.

Boulland JL, Jenstad M, Boekel AJ, Wouterlood FG, Edwards RH, Storm-Mathisen J, Chaudhry FA. 2009. Vesicular glutamate and GABA transporters sort to distinct sets of vesicles in a population of presynaptic terminals. Cereb Cortex 19:241–248.

Burow A, Day HE, Campeau S. 2005. A detailed characterization of loud noise stress: Intensity analysis of hypothalamo-pituitary-adrenocortical axis and brain activation. Brain Res 1062:63–73.

Cameron AA, Khan IA, Westlund KN, Cliffer KD, Willis WD. 1995. The efferent projections of the periaqueductal gray in the rat: a *Phaseolus vulgaris*-leucoagglutinin study. I. Ascending projections. J Comp Neurol 351:568–584.

Campeau S, Watson SJ. 1997. Neuroendocrine and behavioral responses and brain pattern of c-fos induction associated with audiogenic stress. J Neuroendocrinol 9:577–588.

Campeau S, Watson SJ Jr. 2000. Connections of some auditory-responsive posterior thalamic nuclei putatively involved in activation of the hypothalamo-pituitary-adrenocortical axis in response to audiogenic stress in rats: an anterograde and retrograde tract tracing study combined with Fos expression. J Comp Neurol 423:474–491.

Canteras NS, Goto M. 1999. Fos-like immunoreactivity in the periaqueductal gray of rats exposed to a natural predator. Neuroreport 10:413–418.

Canteras NS, Simerly RB, Swanson LW. 1995. Organization of projections from the medial nucleus of the amygdala: a PHAL study in the rat. J Comp Neurol 360:213–245.

Carlson DE, Nabavian AM, Gann DS. 1994. Corticotropin-releasing hormone but not glutamate elicits hormonal responses from the parabrachial region in cats. Am J Physiol 267:R337–R348.

Chan RK, Sawchenko PE. 1994. Spatially and temporally differentiated patterns of c-fos expression in brainstem catecholaminergic cell groups induced by cardiovascular challenges in the rat. J Comp Neurol 348:433–460.

Cheung S, Ballew JR, Moore KE, Lookingland KJ. 1998. Contribution of dopamine neurons in the medial zona incerta to the innervation of the central nucleus of the amygdala, horizontal diagonal band of Broca and hypothalamic paraventricular nucleus. Brain Res 808:174–181.

Cole RL, Sawchenko PE. 2002. Neurotransmitter regulation of cellular activation and neuropeptide gene expression in the paraventricular nucleus of the hypothalamus. J Neurosci 22:959–969.

Collin M, Backberg M, Ovesjo ML, Fisone G, Edwards RH, Fujiyama F, Meister B. 2003. Plasma membrane and vesicular glutamate transporter mRNAs/proteins in hypothalamic neurons that regulate body weight. Eur J Neurosci 18: 1265–1278.

Csaki A, Kocsis K, Halasz B, Kiss J. 2000. Localization of glutamatergic/aspartatergic neurons projecting to the hypothalamic paraventricular nucleus studied by retrograde transport of [^{3}H]D-aspartate autoradiography. Neuroscience 101:637–655.

Cullinan WE, Herman JP, Watson SJ. 1993. Ventral subicular interaction with the hypothalamic paraventricular nucleus: evidence for a relay in the bed nucleus of the stria terminalis. J Comp Neurol 332:1–20.

Cullinan WE, Herman JP, Battaglia DF, Akil H, Watson SJ. 1995. Pattern and time course of immediate early gene expression in rat brain following acute stress. Neuroscience 64:477–505.

Cullinan WE, Helmreich DL, Watson SJ. 1996. Fos expression in forebrain afferents to the hypothalamic paraventricular nucleus following swim stress. J Comp Neurol 368:88–99.

Cunningham ET Jr, Sawchenko PE. 1988. Anatomical specificity of noradrenergic inputs to the paraventricular and supraoptic nuclei of the rat hypothalamus. J Comp Neurol 274:60–76.

Cunningham ET Jr, Bohn MC, Sawchenko PE. 1990. Organization of adrenergic inputs to the paraventricular and supraoptic nuclei of the hypothalamus in the rat. J Comp Neurol 292:651–667.

Daftary SS, Boudaba C, Szabo K, Tasker JG. 1998. Noradrenergic excitation of magnocellular neurons in the rat hypothalamic paraventricular nucleus via intranuclear glutamatergic circuits. J Neurosci 18:10619–10628.

Daftary SS, Boudaba C, Tasker JG. 2000. Noradrenergic regulation of parvocellular neurons in the rat hypothalamic paraventricular nucleus. Neuroscience 96:743–751.

de Menezes RC, Zaretsky DV, Sarkar S, Fontes MA, Dimicco JA. 2008. Microinjection of muscimol into the periaqueductal gray suppresses cardiovascular and neuroendocrine response to air jet stress in conscious rats. Am J Physiol 295:R881–R890.

Decavel C, Van den Pol AN. 1992. Converging GABA- and glutamate-immunoreactive axons make synaptic contact with identified hypothalamic neurosecretory neurons. J Comp Neurol 316:104–116.

Eyigor O, Centers A, Jennes L. 2001. Distribution of ionotropic glutamate receptor subunit mRNAs in the rat hypothalamus. J Comp Neurol 434:101–124.

Eyigor O, Minbay Z, Cavusoglu I, Jennes L. 2005. Localization of kainate receptor subunit GluR5-immunoreactive cells in the rat hypothalamus. Brain Res 136:38–44.

Ezure K. 2004. Respiration-related afferents to parabrachial pontine regions. Respir Physiol Neurobiol 143:167–175.

Floyd NS, Keay KA, Arias CM, Sawchenko PE, Bandler R. 1996. Projections from the ventrolateral periaqueductal gray to endocrine regulatory subdivisions of the paraventricular nucleus of the hypothalamus in the rat. Neurosci Lett 220:105–108.

Fremeau RT Jr, Troyer MD, Pahner I, Nygaard GO, Tran CH, Reimer RJ, Bellocchio EE, Fortin D, Storm-Mathisen J, Edwards RH. 2001. The expression of vesicular glutamate transporters defines two classes of excitatory synapse. Neuron 31:247–260.

Fremeau RT Jr, Burman J, Qureshi T, Tran CH, Proctor J, Johnson J, Zhang H, Sulzer D, Copenhagen DR, Storm-Mathisen J, Reimer RJ, Chaudhry FA, Edwards RH. 2002. The identification of vesicular glutamate transporter 3 suggests novel modes of signaling by glutamate. Proc Natl Acad Sci U S A 99:14488–14493.

Fujiyama F, Furuta T, Kaneko T. 2001. Immunocytochemical localization of candidates for vesicular glutamate transporters in the rat cerebral cortex. J Comp Neurol 435: 379–387.

Furuta A, Martin LJ, Lin CL, Dykes-Hoberg M, Rothstein JD. 1997a. Cellular and synaptic localization of the neuronal glutamate transporters excitatory amino acid transporter 3 and 4. Neuroscience 81:1031–1042.

Furuta A, Rothstein JD, Martin LJ. 1997b. Glutamate transporter protein subtypes are expressed differentially during rat CNS development. J Neurosci 17:8363–8375.

Gauriau C, Bernard JF. 2002. Pain pathways and parabrachial circuits in the rat. Exp Physiol 87:251–258.

Gomez-Flores R, Weber RJ. 2000. Differential effects of buprenorphine and morphine on immune and neuroendocrine functions following acute administration in the rat mesencephalon periaqueductal gray. Immunopharmacology 48: 145–156.

Gras C, Herzog E, Bellenchi GC, Bernard V, Ravassard P, Pohl M, Gasnier B, Giros B, El Mestikawy S. 2002. A third vesicular glutamate transporter expressed by cholinergic and serotoninergic neurons. J Neurosci 22:5442–5451.

Gray TS, Carney ME, Magnuson DJ. 1989. Direct projections from the central amygdaloid nucleus to the hypothalamic paraventricular nucleus: possible role in stress-induced adrenocorticotropin release. Neuroendocrinology 50:433–446.

Hayashi M, Otsuka M, Morimoto R, Hirota S, Yatsushiro S, Takeda J, Yamamoto A, Moriyama Y. 2001. Differentiation-associated Na^+-dependent inorganic phosphate cotransporter (DNPI) is a vesicular glutamate transporter in endocrine glutamatergic systems. J Biol Chem 276: 43400–43406.

Helfferich F, Palkovits M. 2003. Acute audiogenic stress-induced activation of CRH neurons in the hypothalamic paraventricular nucleus and catecholaminergic neurons in the medulla oblongata. Brain Res 975:1–9.

Herman JP, Eyigor O, Ziegler DR, Jennes L. 2000. Expression of ionotropic glutamate receptor subunit mRNAs in the hypothalamic paraventricular nucleus of the rat. J Comp Neurol 422:352–362.

Herman JP, Figueiredo H, Mueller NK, Ulrich-Lai Y, Ostrander MM, Choi DC, Cullinan WE. 2003. Central mechanisms of stress integration: hierarchical circuitry controlling hypothalamo-pituitary-adrenocortical responsiveness. Front Neuroendocrinol 24:151–180.

Herzog E, Gilchrist J, Gras C, Muzerelle A, Ravassard P, Giros B, Gaspar P, El Mestikawy S. 2004. Localization of VGLUT3, the vesicular glutamate transporter type 3, in the rat brain. Neuroscience 123:983–1002.

Hisano S, Hoshi K, Ikeda Y, Maruyama D, Kanemoto M, Ichijo H, Kojima I, Takeda J, Nogami H. 2000. Regional expression of a gene encoding a neuron-specific Na^+-dependent inorganic phosphate cotransporter (DNPI) in the rat forebrain. Brain Res 83:34–43.

Hisano S, Sawada K, Kawano M, Kanemoto M, Xiong G, Mogi K, Sakata-Haga H, Takeda J, Fukui Y, Nogami H. 2002. Expression of inorganic phosphate/vesicular glutamate transporters (BNPI/VGLUT1 and DNPI/VGLUT2) in the cerebellum and precerebellar nuclei of the rat. Brain Res 107: 23–31.

Hrabovszky E, Halasz J, Meelis W, Kruk MR, Liposits Z, Haller J. 2005. Neurochemical characterization of hypothalamic neurons involved in attack behavior: glutamatergic dominance and co-expression of thyrotropin-releasing hormone in a subset of glutamatergic neurons. Neuroscience 133: 657–666.

Hur EE, Zaborszky L. 2005. Vglut2 afferents to the medial prefrontal and primary somatosensory cortices: a combined retrograde tracing in situ hybridization study. J Comp Neurol 483:351–373.

Kainu T, Honkaniemi J, Gustafsson JA, Rechardt L, Pelto-Huikko M. 1993. Co-localization of peptide-like immunoreactivities with glucocorticoid receptor- and Fos-like immunoreactivities in the rat parabrachial nucleus. Brain Res 615:245–251.

Kaneko T, Fujiyama F. 2002. Complementary distribution of vesicular glutamate transporters in the central nervous system. Neurosci Res 42:243–250.

Kaneko T, Fujiyama F, Hioki H. 2002. Immunohistochemical localization of candidates for vesicular glutamate transporters in the rat brain. J Comp Neurol 444:39–62.

Keay KA, Bandler R. 1993. Deep and superficial noxious stimulation increases Fos-like immunoreactivity in different regions of the midbrain periaqueductal grey of the rat. Neurosci Lett 154:23–26.

Keay KA, Bandler R. 2004. Periaqueductal gray. In: Paxinos G, editor. The rat nervous system, 3rd ed. New York: Elsevier. p 243–257.

Keay KA, Li QF, Bandler R. 2000. Muscle pain activates a direct projection from ventrolateral periaqueductal gray to rostral ventrolateral medulla in rats. Neurosci Lett 290: 157–160.

Keay KA, Clement CI, Depaulis A, Bandler R. 2001. Different representations of inescapable noxious stimuli in the periaqueductal gray and upper cervical spinal cord of freely moving rats. Neurosci Lett 313:17–20.

Khan AM, Stanley BG, Bozzetti L, Chin C, Stivers C, Curras-Collazo MC. 2000. N-methyl-D-aspartate receptor subunit NR2B is widely expressed throughout the rat diencephalon: an immunohistochemical study. J Comp Neurol 428: 428–449.

Kiss J, Gorcs TJ, Kuhn R, Knopfel T, Csaky A, Halasz B. 1996. Distribution of metabotropic glutamate receptor 1a in the rat hypothalamus: an immunocytochemical study using monoclonal and polyclonal antibody. Acta Biol Hung 47:221–237.

Kiss J, Halasz B, Csaki A, Liposits Z, Hrabovszky E. 2007. Vesicular glutamate transporter 2 protein and mRNA containing neurons in the hypothalamic suprachiasmatic nucleus of the rat. Brain Res Bull 74:397–405.

Kollack-Walker S, Don C, Watson SJ, Akil H. 1999. Differential expression of c-fos mRNA within neurocircuits of male hamsters exposed to acute or chronic defeat. J Neuroendocrinol 11:547–559.

Krout KE, Loewy AD. 2000. Periaqueductal gray matter projections to midline and intralaminar thalamic nuclei of the rat. J Comp Neurol 424:111–141.

Krukoff TL, Harris KH, Jhamandas JH. 1993. Efferent projections from the parabrachial nucleus demonstrated with the anterograde tracer *Phaseolus vulgaris* leucoagglutinin. Brain Res Bull 30:163–172.

Kugler P, Schmitt A. 1999. Glutamate transporter EAAC1 is expressed in neurons and glial cells in the rat nervous system. Glia 27:129–142.

Li HY, Sawchenko PE. 1998. Hypothalamic effector neurons and extended circuitries activated in "neurogenic" stress: a comparison of foot shock effects exerted acutely, chronically, and in animals with controlled glucocorticoid levels. J Comp Neurol 393:244–266.

Lim LW, Blokland A, van Duinen M, Visser-Vandewalle V, Tan S, Vlamings R, Janssen M, Jahanshahi A, Aziz-Mohammadi M, Steinbusch HW, Schruers K, Temel Y. 2011. Increased plasma corticosterone levels after periaqueductal gray stimulation-induced escape reaction or panic attacks in rats. Behav Brain Res 218:301–307.

Lin W, McKinney K, Liu L, Lakhlani S, Jennes L. 2003. Distribution of vesicular glutamate transporter-2 messenger ribonucleic Acid and protein in the septum-hypothalamus of the rat. Endocrinology 144:662–670.

Mateos JM, Azkue J, Benitez R, Sarria R, Losada J, Conquet F, Ferraguti F, Kuhn R, Knopfel T, Grandes P. 1998.

Immunocytochemical localization of the mGluR1b metabotropic glutamate receptor in the rat hypothalamus. J Comp Neurol 390:225–233.

Michaud DS, McLean J, Keith SE, Ferrarotto C, Hayley S, Khan SA, Anisman H, Merali Z. 2003. Differential impact of audiogenic stressors on Lewis and Fischer rats: behavioral, neurochemical, and endocrine variations. Neuropsychopharmacology 28:1068–1081.

Morilak DA, Barrera G, Echevarria DJ, Garcia AS, Hernandez A, Ma S, Petre CO. 2005. Role of brain norepinephrine in the behavioral response to stress. Prog Neuropsychopharmacol Biol Psychiatry 29:1214–1224.

Motta SC, Goto M, Gouveia FV, Baldo MV, Canteras NS, Swanson LW. 2009. Dissecting the brain's fear system reveals the hypothalamus is critical for responding in subordinate conspecific intruders. Proc Natl Acad Sci U S A 106:4870–4875.

Ni B, Rosteck PR Jr, Nadi NS, Paul SM. 1994. Cloning and expression of a cDNA encoding a brain-specific Na^{+}-dependent inorganic phosphate cotransporter. Proc Natl Acad Sci U S A 91:5607–5611.

Ni B, Wu X, Yan GM, Wang J, Paul SM. 1995. Regional expression and cellular localization of the Na^{+}-dependent inorganic phosphate cotransporter of rat brain. J Neurosci 15: 5789–5799.

Oliver C, Jezova D, Grino M, Paulmyer-Lacroix O, Boudouresque F, Joanny P. 1996. Excitatory amino acid receptors and their localization in the nervous system and hypothalamus. In: Brann DW, Mahesh VB, editors. Excitatory amino acid receptors: their role in neuroendocrine function. New York: CRC Press. p 167–185.

Ozkan ED, Ueda T. 1998. Glutamate transport and storage in synaptic vesicles. Jpn J Pharmacol 77:1–10.

Palkovits M, Dobolyi A, Helfferich F, Usdin TB. 2004. Localization and chemical characterization of the audiogenic stress pathway. Ann N Y Acad Sci 1018:16–24.

Petralia RS, Wenthold RJ. 1996. Types of excitatory amino acid receptors and their localization in the nervous system and hypothalamus. In: Brann DW, Mahesh VB, editors. Excitatory amino acid receptors: their role in neuroendocrine function. New York: CRC Press. p 55–101.

Petrovich GD, Canteras NS, Swanson LW. 2001. Combinatorial amygdalar inputs to hippocampal domains and hypothalamic behavior systems. Brain Res Brain Res Rev 38:247–289.

Prewitt CM, Herman JP. 1998. Anatomical interactions between the central amygdaloid nucleus and the hypothalamic paraventricular nucleus of the rat: a dual tract-tracing analysis. J Chem Neuroanat 15:173–185.

Reilly S. 1999. The parabrachial nucleus and conditioned taste aversion. Brain Res Bull 48:239–254.

Reilly S, Trifunovic R. 2001. Lateral parabrachial nucleus lesions in the rat: neophobia and conditioned taste aversion. Brain Res Bull 55:359–366.

Rinaman L, Hoffman GE, Dohanics J, Le WW, Stricker EM, Verbalis JG. 1995. Cholecystokinin activates catecholaminergic neurons in the caudal medulla that innervate the paraventricular nucleus of the hypothalamus in rats. J Comp Neurol 360:246–256.

Rothstein JD, Martin L, Levey AI, Dykes-Hoberg M, Jin L, Wu D, Nash N, Kuncl RW. 1994. Localization of neuronal and glial glutamate transporters. Neuron 13:713–725.

Sato K, Kiyama H, Tohyama M. 1993. The differential expression patterns of messenger RNAs encoding non-N-methyl-D-aspartate glutamate receptor subunits (GluR1–4) in the rat brain. Neuroscience 52:515–539.

Sawchenko PE, Swanson LW. 1981. Central noradrenergic pathways for the integration of hypothalamic neuroendocrine and autonomic responses. Science 214:685–687.

Sawchenko PE, Swanson LW. 1982. The organization of noradrenergic pathways from the brainstem to the paraventricular and supraoptic nuclei in the rat. Brain Res 257: 275–325.

Sawchenko PE, Swanson LW. 1983. The organization of forebrain afferents to the paraventricular and supraoptic nuclei of the rat. J Comp Neurol 218:121–144.

Sawchenko PE, Benoit R, Brown MR. 1988. Somatostatin 28-immunoreactive inputs to the paraventricular and supraoptic nuclei: principal origin from non-aminergic neurons in the nucleus of the solitary tract. J Chem Neuroanat 1: 81–94.

Sawchenko PE, Brown ER, Chan RK, Ericsson A, Li HY, Roland BL, Kovacs KJ. 1996. The paraventricular nucleus of the hypothalamus and the functional neuroanatomy of visceromotor responses to stress. Prog Brain Res 107:201–222.

Sawchenko PE, Li HY, Ericsson A. 2000. Circuits and mechanisms governing hypothalamic responses to stress: a tale of two paradigms. Prog Brain Res 122:61–78.

Schafer MK, Varoqui H, Defamie N, Weihe E, Erickson JD. 2002. Molecular cloning and functional identification of mouse vesicular glutamate transporter 3 and its expression in subsets of novel excitatory neurons. J Biol Chem 277:50734–50748.

Silveira MC, Sandner G, Graeff FG. 1993. Induction of Fos immunoreactivity in the brain by exposure to the elevated plus-maze. Behav Brain Res 56:115–118.

Smotherman WP, Hennessy JW, Levine S. 1976. Plasma corticosterone levels as an index of the strength of illness induced taste aversions. Physiol Behav 17:903–908.

Spencer CM, Houpt TA. 2001. Dynamics of c-fos and ICER mRNA expression in rat forebrain following lithium chloride injection. Brain Res 93:113–126.

St. Andre J, Albanos K, Reilly S. 2007. C-fos expression in the rat brain following lithium chloride-induced illness. Brain Res 1135:122–128.

Storm-Mathisen J, N.C. D, Ottersen O. 1995. Localization of glutamate and its membrane transport proteins. In: Stone TS, editor. CNS neurotransmitters and neuromodulators: glutamate. New York: CRC Press. p 1–16.

Stornetta RL, Sevigny CP, Guyenet PG. 2002. Vesicular glutamate transporter DNPI/VGLUT2 mRNA is present in C1 and several other groups of brainstem catecholaminergic neurons. J Comp Neurol 444:191–206.

Swanson LW. 1987. Integrated systems of the CNS, part I: hypothalamus, hippocampus, amygdala, retina. In: Bjorklund A, Hokfelt T, Swanson LW, editors. Handbook of chemical neuroanatomy. New York: Elsevier.

Swanson LW. 2004. Brain maps: structure of the rat brain. New York: Elsevier.

Swanson LW, Sawchenko PE. 1983. Hypothalamic integration: organization of the paraventricular and supraoptic nuclei. Annu Rev Neurosci 6:269–324.

Takamori S, Rhee JS, Rosenmund C, Jahn R. 2000. Identification of a vesicular glutamate transporter that defines a glutamatergic phenotype in neurons. Nature 407:189–194.

Takamori S, Malherbe P, Broger C, Jahn R. 2002. Molecular cloning and functional characterization of human vesicular glutamate transporter 3. EMBO Rep 3:798–803.

Tasker JG, Boudaba C, Schrader LA. 1998. Local glutamatergic and GABAergic synaptic circuits and metabotropic glutamate receptors in the hypothalamic paraventricular and supraoptic nuclei. Adv Exp Med Biol 449:117–121.

Ulrich-Lai YM, Jones KR, Ziegler DR, Cullinan WE, Herman JP. 2011. Forebrain origins of glutamatergic innervation to the rat paraventricular nucleus of the hypothalamus: differential inputs to the anterior vs. posterior subregions. J Comp Neurol 519:1301–1319.

Vagg DJ, Bandler R, Keay KA. 2008. Hypovolemic shock: critical involvement of a projection from the ventrolateral periaqueductal gray to the caudal midline medulla. Neuroscience 152:1099–1109.

Van den Pol AN. 1991. Glutamate and aspartate immunoreactivity in hypothalamic presynaptic axons. J Neurosci 11: 2087–2101.

Van den Pol AN, Wuarin JP, Dudek FE. 1990. Glutamate, the dominant excitatory transmitter in neuroendocrine regulation. Science 250:1276–1278.

Van den Pol AN, Hermans-Borgmeyer I, Hofer M, Ghosh P, Heinemann S. 1994. Ionotropic glutamate-receptor gene expression in hypothalamus: localization of AMPA, kainate, and NMDA receptor RNA with in situ hybridization. J Comp Neurol 343:428–444.

Van den Pol AN, Wuarin JP, Dudek FE. 1996. Glutamate neurotransmission in the neuroendocrine hypothalamus. In: Brann DW, Mahesh VB, editors. excitatory amino acid receptors: their role in neuroendocrine function. New York: CRC Press. p 1–54.

Varoqui H, Schafer MK, Zhu H, Weihe E, Erickson JD. 2002. Identification of the differentiation-associated Na^+/PI transporter as a novel vesicular glutamate transporter expressed in a distinct set of glutamatergic synapses. J Neurosci 22:142–155.

Velaz-Faircloth M, McGraw TS, alandro MS, Fremeau RT Jr, Kilberg MS, Anderson KJ. 1996. Characterization and distribution of the neuronal glutamate transporter EAAC1 in rat brain. Am J Physiol 270:C67–C75.

Wagner CK, Eaton MJ, Moore KE, Lookingland KJ. 1995. Efferent projections from the region of the medial zona incerta containing A13 dopaminergic neurons: a PHA-L anterograde tract-tracing study in the rat. Brain Res 677:229–237.

Wang HL, Morales M. 2009. Pedunculopontine and laterodorsal tegmental nuclei contain distinct populations of cholinergic, glutamatergic and GABAergic neurons in the rat. Eur J Neurosci 29:340–358.

Watson RE Jr, Wiegand SJ, Clough RW, Hoffman GE. 1986. Use of cryoprotectant to maintain long-term peptide immunoreactivity and tissue morphology. Peptides 7:155–159.

Whitnall MH. 1993. Regulation of the hypothalamic corticotropin-releasing hormone neurosecretory system. Prog Neurobiol 40:573–629.

Wittmann G, Lechan RM, Liposits Z, Fekete C. 2005. Glutamatergic innervation of corticotropin-releasing hormone- and thyrotropin-releasing hormone-synthesizing neurons in the hypothalamic paraventricular nucleus of the rat. Brain Res 1039:53–62.

Wuarin JP, Dudek FE. 1991. Excitatory amino acid antagonists inhibit synaptic responses in the guinea pig hypothalamic paraventricular nucleus. J Neurophysiol 65:946–951.

Yoshida K, Konishi M, Nagashima K, Saper CB, Kanosue K. 2005. Fos activation in hypothalamic neurons during cold or warm exposure: projections to periaqueductal gray matter. Neuroscience 133:1039–1046.

Ziegler DR, Herman JP. 2002. Neurocircuitry of stress integration: anatomical pathways regulating the hypothalamic-pituitary-adrenocortical axis of the rat. Integr Comp Biol 42: 541–551.

Ziegler DR, Cullinan WE, Herman JP. 2002. Distribution of vesicular glutamate transporter mRNA in rat hypothalamus. J Comp Neurol 448:217–229.

Ziegler DR, Cullinan WE, Herman JP. 2005. Organization and regulation of paraventricular nucleus glutamate signaling systems: N-methyl-D-aspartate receptors. J Comp Neurol 484:43–56.